# Main Manuscript for

Myosin binding protein-C limits strain induced cross-bridge detachment in response to rapid stretch in cardiac and skeletal muscle

Nichlas M. Engels[1], Rachel L. Sadler[2], Michel N. Kuehn[3,4], Devin L. Nissen[5], Dylan Reichert[6], Marius Meinhold[7,8],Wolfgang A. Linke[3], Weikang Ma[5,9,10], Anthony L. Hessel[3,4], and Samantha P. Harris[2]*

[1]Department of Cellular and Molecular Medicine, University of Arizona, Tucson, AZ

[2]Department of Physiology, University of Arizona, Tucson, AZ

[3]Institute of Physiology II, University of Muenster, Muenster, Germany

[4]Accelerated Muscle Biotechnologies, Mansfield, MA, USA

[5]BioCAT, Department of Biology, Illinois Institute of Technology, Chicago, IL, USA

[6]Department of Biomedical Engineering, University of Arizona, Tucson, AZ, USA

[7]Department of Comparative Biosciences, University of Wisconsin–Madison, Madison, WI, USA.

[8]School of Veterinary Medicine, University of Wisconsin–Madison, Madison, WI, USA.

[9]Center for Synchrotron Radiation Research and Instrumentation, Illinois Institute of Technology, Chicago, IL, USA

[10]Pritzker Institute of Biomedical Science and Engineering, Illinois Institute of Technology, Chicago, IL, USA

* Samantha P. Harris

**Email:** samharris@arizona.edu

**Author Contributions:** N.M.E, A.L.H, and S.P.H conceptualized the project, , N.M.E conducted the investigation, N.M.E visualized the datasets, S.P.H was the project administrator, A.L.H, and S.P.H supervised the study, N.M.E wrote the original draft, all authors reviewed, edited, and agreed to the final draft.

**Competing Interest Statement:** W.M. consults for Edgewise Therapeutics, Cytokinetics Inc. and Kardigan Bio, but these activities have no relation to the current work. A.L.H. and M.N.K. are founders and owners of Accelerated Muscle Biotechnologies, but that work is not related to the current project. All other authors declare no competing interests.

**Classification:**

Biological Sciences (Major)

Minor; Physiology

**Keywords:** myosin binding protein-C, stretch activation, cross-bridge kinetics, mouse models

**Abstract**

Myosin binding protein-C (MyBP-C) consists of a family of regulatory proteins expressed in sarcomeres of cardiac, fast and slow twitch skeletal muscles. The 3 MyBP-C paralogs expressed in each muscle type are encoded by separate genes but maintain a similar structure. Given the overall similarity in structure and localization of each of paralog, it is assumed that MyBP-C expressed in different muscles have similar functional effects. Here we directly tested this assumption by making use of our cut and paste approach to remove and replace N-terminal regions of MyBP-C in sarcomeres of different muscle types. We found that the different MyBP-C paralogs similarly slowed cross-bridge cycling kinetics, increased $Ca^{2+}$ sensitivity of tension, and damped force oscillations. However, responses to a rapid stretch in actively contracting fibers, taken as indices of cross-bridge detachment and attachment kinetics, differed in each muscle type and responses depended on the presence or absence of a given paralog of MyBP-C. Altered responses to stretch were most evident for fast MyBP-C where loss of MyBP-C in psoas muscle resulted in transient responses to stretch that resembled those found in cardiomyocytes. Replacement of cardiac MyBP-C with fast MyBP-C in cardiomyocytes led to responses similar to psoas muscle. In separate X-ray diffraction experiments we also found that loss of MyBP-C in $Ca^{2+}$-activated psoas muscle increased lattice disorder, reduced the ordering of myosin heads, and decreased thin filament length. Taken together, these results indicate that the different MyBP-C paralogs exert both common and unique effects on myosin cross-bridge kinetics.

**Significance Statement**

MyBP-C is a family of regulatory proteins found in muscle sarcomeres, where they regulate contraction and relaxation. Mutations in all MyBP-C paralogs cause disease in

skeletal and cardiac muscles. We used a powerful “cut and paste” strategy to selectively remove MyBP-C from slow-twitch, fast-twitch, and cardiac muscle to show that each MyBP-C effects cross-bridge behavior similarly, though to varying degrees. Each MyBP-C had a notable effect on transient responses to rapid stretch, where MyBP-C was found to limit strain-induced cross-bridge detachment, especially in fast-twitch muscles. Strain-induced cross-bridge detachment is critical for rapid filling of the left ventricle in diastole and for sustained contraction in skeletal muscle. MyBP-C paralogs appear adapted to meet the mechanical demands of each muscle type.

## Main Text

### Introduction

Myosin binding protein-C (MyBP-C) consists of a family of regulatory proteins located in sarcomeres of striated muscle. Within this family, there exist three unique paralogs of MyBP-C, each encoded by a separate gene and expressed in specific fiber types. *Mybpc1* encodes the slow twitch skeletal paralog (sMyBP-C), *Mybpc2* encodes the fast twitch skeletal paralog (fMyBP-C), and *Mybpc3* encodes the cardiac paralog (cMyBP-C)(1) The three paralogs share significant structural homology, as they all consist of a chain of 7 immunoglobulin (Ig)-like domains and 3 fibronectin type III domains termed C1-C10, a regulatory motif referred to as the M-domain, and a proline/alanine-rich domain near the N-terminus(1). Cardiac (cMyBP-C) contains an additional 8$^{th}$ Ig-like domain at the N-terminus termed C0 (Figure 1). Each paralog is located in the C-zone of sarcomeres, where C-terminal domains C8-C10 anchor MyBP-C to the thick filament backbone and interact with myosin heads of crown 1 and 3 in relaxed muscle(2, 3). The N-terminal domains (C0-C2 for cardiac and C1-C2 for skeletal) interact with both thin and thick filaments(4-7). For example, N-terminal interactions with the thin filament shift the

91 tropomyosin cable from the closed to the blocked state, thus promoting activation (i.e.
92 cross-bridge formation) in the presence of $Ca^{2+}$ or delaying relaxation as $Ca^{2+}$ falls(8, 9).
93 In contrast, N-terminal domain interactions with the thick filament have an inhibitory effect
94 on myosin heads by stabilizing myosin heads in the OFF state(10, 11). While less is known
95 regarding the middle domains (C3-C7) of MyBP-C, recent evidence suggests they play a
96 critical auto-inhibitory role limiting the effects of N-terminal domains to activate the thin
97 filament(12, 13). However, neither the position of the N-terminal domains nor the middle
98 domains were resolved in recent cryo-EM reconstructions and so the structural orientation
99 and interactions of these domains in the sarcomere are still unclear.

100 As evidence for MyBP-C's structural and regulatory roles in the sarcomere, mutations in
101 all three MyBP-C genes lead to disease in their respective muscle types. For instance,
102 mutations in *Mybpc3* are a leading cause of hypertrophic cardiomyopathy (HCM)(14-16),
103 while mutations in *Mybpc1* and *Mybpc2* are linked to distal arthrogryposis (DA1) and
104 myogenic muscle tremors(17-19). Although the three proteins share significant structural
105 homology, sequence homology between the paralogs is low, sharing only ~39% sequence
106 identity between the three paralogs in human muscles(20). Additionally, sMyBP-C exists
107 as a subfamily of multiple splice variants which likely have significant functional differences
108 that have yet to be thoroughly characterized(21).

109 Here we sought to compare the relative structural and functional effects of the 3 main
110 MyBP-C paralogs using our cut and paste approach to systematically remove and replace
111 MyBP-C in each of the different muscle types. The approach used 3 lines of gene-edited
112 mice, referred to as $SpyC_1$, $SnoopC_2$, and $SpyC_3$, that allow selective removal and
113 replacement of MyBP-C in slow twitch skeletal, fast twitch skeletal, and cardiac muscles,
114 respectively (Figure 1)(13, 22-24). The unique strength of these mouse models is that they

115 allow for a direct investigation of both the structural and mechanical role of MyBP-C within
116 a single fiber type, where MyBP-C can be selectively removed and replaced in a single,
117 healthy muscle fiber after it has been isolated from the animal. This is because all 3 mouse
118 lines contain a tobacco etch virus (TEV) protease recognition site followed by either a
119 short SpyTag or SnoopTag sequence between domains C7 and C8(22, 23, 25, 26)
120 (Supplemental Figure 1). Upon treatment of permeabilized muscle fibers with TEV
121 protease (TEVp), the endogenous domains C1-C7 in skeletal muscle and C0-C7 in
122 cardiac muscle are selectively cleaved and eliminated from the muscle, while domains
123 C8-C10 remain anchored to the thick filament. Following cleavage of MyBP-C, added
124 recombinant proteins containing a cognate SpyCatcher (Sc) or SnoopCatcher(SnC) form
125 a spontaneous covalent bond with the SpyTag or SnoopTag encoded at the N-terminus
126 of C8, thus permitting covalent ligation ("paste") of any desired recombinant protein *in situ*
127 at the position of endogenous MyBP-C in the sarcomere (Figure 1).

128 Using these gene-edited mouse lines, we performed permeabilized muscle mechanics to
129 measure changes in isometric force, cross-bridge cycling and stretch activation, as well
130 as small-angle X-ray diffraction to identify structural changes to the sarcomere during
131 isometric contraction. Here, we found that each MyBP-C paralog shares certain functional
132 effects including sensitizing myofilaments to $Ca^{2+}$, slowing cross-bridge cycling kinetics,
133 and damping force oscillations at submaximal $Ca^{2+}$ activation. However, we found that
134 each paralog differentially regulates tension responses following a quick stretch,
135 apparently by differentially affecting strain-induced cross-bridge detachment. In psoas
136 muscle these changes correlated with increased thick and thin filament disorder during
137 half-maximal isometric contraction.

138
139 **Results**
140
141 **MyBP-C enhances $Ca^{2+}$-sensitivity of tension and limits cross-bridge**
142 **redevelopment rates ($k_{tr}$) in cardiac muscle and fast twitch and slow twitch muscles**

143 To determine the contribution of each MyBP-C paralog to function in the different muscle
144 fiber types (cardiac, fast skeletal, and slow skeletal), we first investigated the effect of the
145 different MyBP-C paralogs on steady state $Ca^{2+}$-sensitivity of tension as well as the rate
146 of cross-bridge cycling. Both $Ca^{2+}$-sensitivity and crossbridge cycling, the latter of which is
147 indicated by tension recovery from a slack-restretch maneuver, ($k_{tr}$)(27) are both two
148 parameters that are frequently altered under disease conditions. For these experiments,
149 each MyBP-C paralog was selectively cleaved in cardiac left ventricle, fast twitch psoas,
150 and slow twitch soleus muscles from $SpyC_3$, $SnoopC_2$, and $SpyC_1$ mice, respectively, by
151 incubating permeabilized muscle fibers with TEV protease (TEVp). Results shown in
152 Figure 2 demonstrate that loss of the N'-terminal domains caused a rightward shift of the
153 tension-pCa curve, indicating reduced $Ca^{2+}$-sensitivity of tension such that higher [$Ca^{2+}$] is
154 required to achieve a given amount of force. In $SpyC_3$ cardiac muscle the $pCa_{50}$ for tension
155 (where pCa50=-log[$Ca^{+}$]) was shifted from 5.401 ± 0.01 prior to TEVp treatment to
156 5.32 ± 0.01 after treatment (n=13, $p < 0.001$) (Figure 2a). Similarly, in $SnoopC_2$ fast twitch
157 psoas muscle, the $pCa_{50}$ was shifted from 5.63 ± 0.01 to 5.57 ± 0.01, (n=10, $p < 0.001$)
158 (Figure 2b). In $SpyC_1$ slow twitch soleus we did not observe a change in $Ca^{2+}$-sensitivity.
159 (5.38 ± 0.02 to 5.36 ± 0.02,n=8, n.s) (Figure 2c). However, since mouse soleus muscle
160 expresses a near even mixture of slow and fast twitch fiber type populations with variable
161 MyBP-C paralogs, (28) the lack of a significant difference in $Ca^{2+}$-sensitivity of tension for
162 soleus muscle may reflect a relatively low proportion of sMyBP-C relative to total MyBP-
163 C. However, $k_{tr}$ was faster at sub-maximal levels of $Ca^{2+}$ activation in all 3 muscle types,

164 indicating an increase in cross-bridge cycling rates at these [$Ca^{2+}$] (Figure 2d-f). The
165 increased cycling suggests a change in either cross-bridge attachment or detachment
166 rates.

167 **Loss of MyBP-C promotes the occurrence of spontaneous oscillatory contractions**
168 **(SPOC) in all muscle types.**

169 Another common observation identified in each muscle type following cleavage of MyBP-
170 C by TEVp was the appearance of spontaneous oscillatory contractions (SPOC) that
171 became evident during $Ca^{2+}$-activated contraction(29). The SPOC oscillations are evident
172 as waves of contraction and relaxation that occur spontaneously, i.e., without cyclic
173 changes in activating $Ca^{2+}$ (see Supplemental Videos 1 and 2). Recently, the SPOC
174 phenomenon has been proposed as an underlying mechanism of myogenic tremor in
175 certain skeletal myopathies linked to mutations in MyBP-C(19). We have also previously
176 reported SPOC behavior in detergent-permeabilized cardiomyocytes from $SpyC_3$ left
177 ventricles that had been treated with TEVp to remove the C0-C7 domains of cardiac
178 MyBP-C. Importantly, the oscillations were specifically due to loss of cMyBP-C because
179 they were eliminated by ligation of recombinant cMyBP-C(22). Here we investigated
180 whether SPOC is a common phenomenon following removal of MyBP-C in both slow and
181 fast twitch muscles in addition to cardiomyocytes. Figure 2g-i shows raw force traces from
182 submaximal $Ca^{2+}$-activated force contractions in cardiac tissue from $SpyC_3$, in psoas
183 muscles from $SnoopC_2$ mice and in soleus muscle from $SpyC_1$ mice before and after
184 treatment with TEVp. Results show that removal of C1-C7 domains from both $SnoopC_2$
185 psoas and $SpyC_1$ soleus muscle consistently resulted in robust SPOC behavior which was
186 evident as force overshoots and instabilities in the raw force traces during $Ca^{2+}$ activation
187 (see also Supplemental videos S1 and S2). Similar to SPOC observed in cardiomyocytes,

188 SPOC in skeletal fibers occurred most commonly at submaximal [$Ca^{2+}$] near the $pCa_{50}$ for
189 force generation. Therefore, MyBP-C paralogs appear critical in preventing SPOC from
190 occurring in both cardiac and skeletal muscles where undamped or prolonged SPOC may
191 contribute to muscle dysfunction in disease.

192

193 **MyBP-C paralogs differentially regulate muscle responses to rapid stretch during**
194 **$Ca^{2+}$ activation**

195 We next investigated whether MyBP-C affects rapid tension responses following stretch
196 in $Ca^{2+}$ activated fibers because these responses give insights into cross-bridge
197 detachment/attachment events as well as the delayed recovery of force referred to as SA.
198 For these experiments, muscles were subjected to a rapid 2% stretch relative to initial
199 muscle length followed by a 3 sec hold at the new length before returning to the initial
200 length. The resulting transient responses to the acute stretch are typically interpreted in
201 terms of cross-bridge behaviors(30, 31). As shown in Figure 3, the overall shape of the
202 resulting tension transients in response to quick stretch varied significantly depending on
203 the muscle type (i.e., responses to rapid stretch differed in cardiac, slow twitch, or fast
204 twitch skeletal muscles).

205 Figure 1 shows representative traces from cardiac muscle and psoas muscle that
206 illustrate the 3 typical phases of the transient force responses to stretch. In cardiac muscle
207 following rapid stretch there is a rapid increase in force ($P_1$) that coincides with and is
208 proportional to the initial stretch/increase in length. $P_1$ is related to both strain on bound
209 cross-bridges as well as strain on elastic elements within the sarcomere, such as titin(32).
210 Following the $P_1$ peak, the force drops rapidly in such a way that the rate of the decrease

211 in tension ($K_{rel}$) is related to the kinetics of cross-bridge detachment. Next, the nadir of the
212 tension decrease is termed $P_2$ and typically approaches or drops below the pre-stretch
213 steady state tension (33). Following $P_2$, there is a delayed rise in tension where tension
214 increases to a new steady-state value that is greater than the pre-stretch steady state
215 force ($P_3$). This rise to a new steady state force ($P_3$) termed SA (33-35), is most prominent
216 in muscles that do oscillatory work such as some insect flight muscles and vertebrate
217 cardiac muscle, whereas it is typically less prominent and shorter lived in skeletal
218 muscle(34, 36). In fast twitch skeletal muscle, the rapid increase to P1 is similar to cardiac
219 muscle. However, there is a notable difference following the initial relaxation between
220 cardiac and fast twitch skeletal muscle, where $P_2$ typically remains greater than the steady
221 state force prior to stretch(34). Next, instead of a delayed rise in tension to a new steady
222 state ($P_3$), the force briefly plateaus before slowly decreasing to a steady-state. Since the
223 fast twitch muscle tension transient typically lacks a delayed regeneration of force, the SA
224 response is considered minimal in fast twitch skeletal muscle.

225 Here, we found that the tension responses to rapid stretch were affected following removal
226 of MyBP-C in each muscle, albeit, to varying degrees. A representative trace for each
227 muscle type before and after removal of MyBP-C is shown in Figure 3. Results show that
228 removal of cMyBP-C in cardiomyocytes had overall modest effects on tension transients,
229 i.e. loss of cMyBP-C slightly reduced the $P_2$ nadir (by ~4% at pCa 4.5 and 5.2), increased
230 the $P_{df}$ amplitude ($P_3$-$P_2$) by ~4% at $pCa_{50}$, and increased $k_{rel}$, the rate of relaxation
231 following the $P_1$ peak (97.56 ± 7.37 to 129.37 ± 8.20 at $pCa_{50}$) (Fig. 3d,g,j). However,
232 effects of removing fMyBP-C in psoas muscle were much more profound where tension
233 transients following loss of fMyBP-C (Figure 3b) now closely resembled a typical transient
234 response seen in cardiac muscle. That is, removal of fMyBP-C significantly decreased the

235 $P_2$ nadir below the pre-stretch steady state and increased the $P_{df}$ amplitude. $K_{rel}$ was also
236 significantly increased at sarcomere length (SL) 3.0 (Supplementary Figure 2), although
237 $K_{rel}$ remained unchanged at SL 2.4 possibly due to a lower rate of data acquisition for this
238 data set (Figure 3e,h,k). Most strikingly, the acute removal of fMyBP-C resulted in the
239 appearance of a new delayed phase of force regeneration (phase 3) that is usually minimal
240 or absent in fast twitch fibers. This was primarily due to the decrease in $P_2$ because the
241 $P_3$ amplitudes remained unchanged in cardiac and skeletal muscle. However, the P3 does
242 appear slightly increased in the presence of fMyBP-C (Supplemental Figure 3). In slow
243 twitch soleus muscle, similar to cardiac muscle, the overall shape of the transient was not
244 dramatically changed following loss of sMyBP-C, but both the $P_2$ nadir decreased further
245 beyond the pre-stretch steady state, $P_{df}$ amplitude increased, and $K_{rel}$ rates were also
246 increased (Figure 3f,i,l). Taken together, loss of fMyBP-C conferred SA-like properties to
247 fast skeletal fibers, suggesting that canonical cross-bridge tension transient responses to
248 stretch are modulated by MyBP-C paralogs in the different fiber types.

249

250 **Skeletal muscle MyBP-C paralogs alter tension transient properties in cardiac**
251 **muscle.**

252 To directly test the extent to which differences in transient tension responses to stretch
253 are due to MyBP-C paralog expression in different muscle types, we next assessed
254 whether fMyBP-C and sMyBP-C could confer skeletal-like responses to stretch in
255 cardiomyocytes. We chose cardiac muscle as the background for paralog exchanges in
256 this set of experiments because we were able to remove nearly all endogenous cMyBP-
257 C following TEV protease treatment in cardiac myocytes compared with the more limited
258 removal of skeletal muscle paralogs from either psoas or soleus muscles that express a

259 mixture of skeletal MyBP-C paralogs (22). Additionally, because mouse hearts contain
260 primarily a single myosin isoform ($\alpha$-myosin)(37), other potentially confounding effects due
261 to variable myosin isoform expression in different skeletal muscle fiber types are
262 avoided(38). Therefore, to directly assess effects of the different MyBP-C paralogs,
263 cardiomyocytes from $SpyC_3$ mice were first treated with TEVp to eliminate endogenous
264 cMyBP-C and then cMyBP-C was replaced *in situ* with either recombinant cMyBP-C,
265 fMyBP-C or sMyBP-C via SpyCatcher encoded at their C'-terminal ends. As shown in
266 Figure 5a, recombinant cMyBP-C was first added as control. Ligation of recombinant
267 cardiac C0C7Sc did not alter the overall shape of the tension transient compared to before
268 TEVp treatment, although the $P_2$ value tended to be higher. This could be due to the lack
269 of post-translational modifications (e.g., phosphorylation) of the recombinant C0C7Sc
270 compared to the endogenous cMyBP-C prior to TEVp treatment since phosphorylation of
271 cMyBP-C reduces $P_2$(39). Ligation of cardiac C0C7Sc also restored $Ca^{2+}$-sensitivity of
272 tension ($pCa_{50}$: Pre: 5.41 ± 0.01, Post: 5.32 ± 0.01, cC0C7Sc: 5.39 ± 0.02) and reduced
273 $k_{tr}$ rates to values before treatment with TEVp (Figure 4a,d). Similar effects were observed
274 for ligation of fast C1C7Sc, where $Ca^{2+}$-sensitivity was restored ($pCa_{50}$: Pre:5.54 ± 0.02,
275 Post:5.44 ± 0.01, fC1C7Sc: 5.54 ± 0.01) (Fig. 4.b,e). However, after ligation of fC1C7Sc
276 transient responses to stretch in cardiac muscle were altered such that they more closely
277 resembled those typically seen in fast twitch skeletal fibers instead of those seen in
278 cardiomyocytes. That is, fC1C7Sc significantly elevated the $P_2$ amplitude above the pre-
279 stretch steady state force and nearly eliminated the rise in $P_3$ force (SA), leading to
280 negative $P_{df}$ values (Figure 5e,h). Additionally, fC1C7Sc decreased the phase 2 relaxation
281 rate $K_{rel}$, trending to be slightly slower than endogenous cMyBP-C. (Fig. 5k). Taken
282 together, these experiments demonstrate that removal of fMyBP-C from psoas muscle
283 altered the tension transient to resemble cardiac muscle, while addition of recombinant

284 fC1C7Sc to cardiac muscle altered the tension transient to resemble fast twitch skeletal
285 muscle.

286 Similar results were seen following replacement with sC1C7Sc, which was able to restore
287 $Ca^{2+}$-sensitivity of tension ($pCa_{50}$: Pre 5.55 ± 0.02. Post: 5.49 ± 0.01, sC1C7Sc: 5.54 ±
288 0.02) and reduce $k_{tr}$ rates to a similar extent as addition of cMyBP-C (Figure 4c,f).
289 Therefore, both recombinant fMyBP-C and sMyBP-C are sufficient to restore typical
290 interactions of endogenous cMyBP-C in cardiac muscle. sC1C7Sc also raised the $P_2$ nadir
291 to a level above pre-stretch steady state and nearly eliminated $P_{df}$ amplitude of the tension
292 transient, thus significantly blunting the SA response typically seen in cardiac muscle (Fig.
293 5f,i). Taken together, these results demonstrate that skeletal muscle paralogs of MyBP-C
294 reduce canonical SA responses in cardiac muscle and instead confer skeletal-like
295 responses to rapid stretch.

296 **Structural changes following loss of fMyBP-C determined by X-ray diffraction**

297 The startling result that fMyBP-C cleavage in psoas leads to cardiac-like SA properties
298 encouraged us to identify underlying sarcomere-level structural changes. We therefore
299 used the small-angle X-ray diffraction technique on permeabilized psoas fibers from
300 $SnoopC_2$ mice under $Ca^{2+}$-activated conditions to determine structural changes in the
301 sarcomere before and after cleavage of fMyBP-C. In particular, we sought to determine
302 whether fMyBP-C contributed to changes in lattice spacing, lattice order, and mass
303 distributions on the thick or thin filaments that could potentially account for the change in
304 transient force behaviors described above. X-ray reflections and their relationship to
305 sarcomere structures can be visualized in the cross-sectional diagram of the sarcomere
306 (Fig. 6a,b,c).

307

308 **fMyBP-C stabilizes lattice order during isometric contraction, reduces myosin**
309 **head order, and shortens thin filament length during isometric contraction**

310 Figure 6 shows a representative X-ray diffraction pattern collected from active SnoopC$_2$
311 psoas muscle. We report on features of equatorial reflections, including the spacing of the
312 1,0 reflection (d10), the thick-filament only lattice plane spacing, and its width in equatorial
313 space, which represents the degree of heterogeneity in the lattice and thick filament
314 disorder ($\sigma_D$)(40). Under activating conditions at pCa 6.0 (approximately the pCa$_{50}$ for
315 force generation), we found that lattice spacing decreased with increasing SL as expected.
316 However, there were no significant differences in lattice spacing following removal of
317 fMyBP-C (Fig. 6d). This result differs from the increase in lattice spacing following loss of
318 fMyBP-C observed under relaxing conditions (23), but may be explained by the relatively
319 greater influence of strongly bound cross-bridges to act on the thin filament and limit lattice
320 expansion during $Ca^{2+}$ activation. However, we found that the heterogeneity of lattice
321 spacing ($\sigma_D$) was significantly increased at both SL 2.4 and 3.0 following removal of
322 fMyBP-C (Fig. 6f). The latter suggests a modest degradation in the lattice integrity during
323 contraction when fMyBP-C is cleaved.

324 In order to further investigate the role of fMyBP-C in the orientation and order of myosin
325 heads as well as the thin filament, we investigated the $I_{1,1}/I_{1,0}$ equatorial intensity ratio and
326 M3, T3, M6 meridional reflections as well as the 6$^{th}$ actin layer line (ALL6) in the X-ray
327 diffraction patterns. The ratio of the 1,0 and 1,1 reflection intensities ($I_{1,1}/I_{1,0}$) reflects the
328 distribution of mass between thick and thin filaments, where increases are typically
329 associated with a shift of myosin heads to the ON state and/or binding of myosin heads to
330 the thin filament. We found that a loss of fMyBP-C did not have a significant effect on the

331 $I_{1,1}/I_{1,0}$ intensity ratio during contraction, suggesting that loss of fMyBP-C did not
332 significantly affect the distribution of myosin heads away from the thick filament backbone
333 or proportion of bound crossbridges under $Ca^{2+}$ activated conditions. The $I_{1,1}/I_{1,0}$ intensity
334 ratios at both short and long SL (SL 2.4 and 3.0) also remained unchanged during
335 isometric contraction, as previously reported by others (41, 42). Next, the spacing of the
336 M3 reflection ($S_{M3}$), a measure of the axial periodicity of myosin heads, did not significantly
337 change at either SL 2.4 or 3.0 following loss of fMyBP-C (Supplementary Figure x).
338 Because $S_{M3}$ is also taken as a measure of whether myosin heads are primarily in the OFF
339 or ON state, results suggest that fMyBP-C does not contribute significantly to the OFF/ON
340 distribution of myosin heads or numbers of bound myosin heads under active conditions,
341 consistent with the $I_{1,1}/I_{1,0}$ intensity ratio. The intensity of the M3 reflection ($I_{M3}$), however,
342 decreased following removal of fMyBP-C (Figure 7g), consistent with an increase in the
343 angular dispersion of myosin heads(43, 44), suggesting that loss of fMyBP-C promotes
344 disorder of myosin heads. The spacings of other thick filament reflections, such as ($S_{M6}$),
345 indicative of thick filament length, were unchanged following removal of fMyBP-C
346 (Supplementary Figure 4).

347 Finally, we sought to determine whether any thin filament structural changes occurred
348 following fMyBP-C removal. We found that the spacing of the third-order troponin reflection
349 ($S_{T3}$) was significantly decreased following removal of fMyBP-C at both SL 2.4 and SL 3.0,
350 suggesting a reordering of the troponin complex on the thin filament. Additionally, the
351 spacing of actin layer line 6 ($S_{ALL6}$), reflecting the pitch left-handed helix of actin, was
352 significantly decreased following removal of fMyBP-C at both SL 2.4 and SL 3.0 μm (Fig.
353 6i).

354
355 **Discussion**

356
357 **Myosin binding protein-C paralogs commonly influence $Ca^{2+}$-sensitivity, cross-**
358 **bridge cycling, and oscillatory contractions in striated muscles**

359 In this study, we sought to identify key similarities and differences in the role of the three
360 major MyBP-C paralogs in regulating muscle contractility, as well as identify key roles for
361 fMyBP-C in the structural organization of isometrically contracting sarcomeres. Using
362 three genetically modified mouse lines specific to slow ($SpyC_1$), fast ($SnoopC_2$), and
363 cardiac-MyBP-C ($SpyC_3$) that allow for selective removal of MyBP-C and replacement with
364 recombinant MyBP-C in the respective muscle types, we were able to test mechanical
365 properties of each muscle type in the presence and absence of MyBP-C. We found that
366 selective cleavage of MyBP-C led to a reduction in $Ca^{2+}$-sensitivity in both cardiac and fast
367 twitch myocytes. Effects on $Ca^{2+}$-sensitivity did not reach significance in soleus, a
368 predominantly slow twitch muscle, likely due to significant co-expression of fast and slow
369 MyBP-C (since fMyBP-C would not be cleaved in skeletal muscles from $SpyC_1$ mice).
370 However, recombinant slow MyBP-C was able to restore $Ca^{2+}$-sensitivity when added to
371 $SpyC_3$ cardiac myocytes (Figure 4f), so all 3 paralogs apparently share the common ability
372 to shift the tension-pCa relationship to the left. Similarly, cleavage of each MyBP-C paralog
373 increased cross-bridge cycling rates at submaximal $Ca^{2+}$ activation as measured by $k_{tr}$.
374 This result is in good agreement with previously reported changes in both cardiac and fast
375 skeletal MyBP-C KO mice as well as previous work with the $SnoopC_2$ and $SpyC_3$ mouse
376 lines(22, 45, 46). Moreover, loss of each MyBP-C paralog led to the appearance of
377 spontaneous oscillatory contractions at sub-maximal $Ca^{2+}$ activations near the $pCa_{50}$ for
378 force generation. While the precise mechanisms by which oscillatory contractions are
379 induced and propagated are still unclear, the phenomenon is an intrinsic, emergent
380 property of sarcomeres that has been likened to a third state of muscle activity between

381 activation and relaxation(29, 47). Notably, because force oscillations occur at $Ca^{2+}$
382 concentrations expected to be encountered in living muscle and are influenced by
383 metabolites such as ADP/$P_i$(48), tension instabilities are likely to have physiological
384 relevance. Consistent with this idea, mutations in slow MyBP-C lead to force oscillations
385 that are associated with skeletal muscle tremor in humans(17, 49, 50). Results presented
386 here therefore suggest that a novel functional role of all 3 MyBP-C paralogs is to limit
387 mechanical force instabilities and promote contractile synchrony. Conversely, loss of
388 MyBP-C or mutations in MyBP-C underlie contractile dysfunction in different muscle types
389 (51).

390 **Myosin Binding Protein C paralogs differentially contribute to tension transients in**
391 **striated muscle**

392 While we identified several common functional effects of the different MyBP-C
393 paralogs as discussed above, a notable departure from this trend was evident when
394 comparing the differential responses to a rapid 2% stretch in each muscle type which we
395 found were attributable to expression of the different MyBP-C paralogs. For instance,
396 under control conditions all 3 muscle types (cardiac, fast and slow skeletal) had unique
397 responses to rapid stretch that were mostly stereotypical for that muscle type as previously
398 described by others(19, 33, 34, 52, 53). This was most evident when comparing the
399 responses of cardiac and psoas (fast skeletal) muscles, where cardiac muscle exhibited
400 a canonical 3 phase response that included a final phase such that after reaching a nadir
401 ($P_2$), steady state force rises above the pre-stretch force, $P_3$. (SA, discussed in more detail
402 below). By contrast, $P_2$ was highly elevated in psoas muscle and the phase 3 rise in force
403 was typically minimal and/or short-lived. Notably, classical SA behavior is generally
404 considered minimal or absent in fast twitch muscle, although enhancement of SA in

405 skeletal muscles may be important under conditions of fatigue (e.g., high inorganic $P_i$) (34,
406 52, 54). Strikingly, as shown in Figure 3, we found that loss of fMyBP-C after TEVp
407 cleavage in psoas muscle completely altered the stereotypical response to stretch and
408 completely converted the response into one resembling that of cardiac muscle, including
409 a significant decrease in $P_2$ and the appearance of a prominent phase 3 SA (delayed force
410 increase) response. Conversely, when fMyBP-C was added to cardiac myocytes (Fig. 5),
411 the tension transient converted into a response more closely resembling one typically
412 found in fast skeletal muscle where $P_2$ was elevated and phase 3 was eliminated. Taken
413 together, our results provide compelling evidence that the different MyBP-C paralogs
414 contribute significantly to the stereotypical tension transient responses in their respective
415 muscle types. Furthermore, to our knowledge, this is the first report showing that loss of
416 fMyBP-C confers classic SA-like properties to fast twitch skeletal muscle fibers.

417 Tension transient responses to stretch, including SA responses, are thought to be
418 mediated largely by changes in cross-bridge cycling kinetics (30). Accordingly, numerous
419 factors that are known to impact cross-bridge dynamics, including calcium, ADP, and $P_i$
420 concentration, the extent of stretch, temperature, and the contribution of other sarcomere
421 proteins, such as thin filament proteins as well as myosin heavy chain isoforms, have all
422 have been shown to significantly impact the shape and rate of tension transient responses
423 to stretch(34, 54-56). In this respect, it may not be surprising that MyBP-C, known to affect
424 cross-bridge cycling kinetics, also influences tension transients. Indeed, consistent with
425 results reported here, Stelzer et al (2006) reported increased $K_{rel}$, reduced $P_2$, and
426 increased $K_{df}$ rates in cMyBP-C KO mice, effects that were largely replicated by PKA
427 phosphorylation of WT cMyBP-C (33, 39). PKA phosphorylation of sMyBP-C in slow twitch
428 fibers also increased force development rates (57). Our results thus confirm and extend

429 previous findings by showing that all 3 MyBP-C paralogs limit cross-bridge cycling kinetics
430 in their respective muscle types. However, to further explore the extent to which each
431 paralog by itself was sufficient to determine the overall shape of tension transients when
432 expressed in a similar background, we also utilized the $SpyC_3$ cardiac mouse line that
433 primarily expresses a single myosin isoform (α-myosin) in cardiac myocytes to
434 systematically replace endogenous cMyBP-C with recombinant cardiac, slow , and fast
435 MyBP-C. Again, we found that each MyBP-C paralog conferred a characteristic tension
436 transient in cardiac muscle, thus allowing us to attribute observed changes in the tension
437 transients primarily to the different paralogs of MyBP-C rather than to different myosin
438 isoforms or other confounding variables.

439 **MyBP-C paralogs determine the extent of strain-induced cross-bridge detachment,**
440 **$P_2$**

441 A key difference that emerged when comparing the tension transients in the different
442 muscle types was the extent of the $P_2$ nadir, which presumably reflects the magnitude of
443 cross-bridge detachment in response to strain in each muscle type. Notably, $P_2$ was
444 reduced following loss of MyBP-C in all 3 muscle types, suggesting that a normal function
445 of MyBP-C is to limit strain-induced cross-bridge detachment. In cardiac muscle, strain-
446 dependent cross-bridge detachment is emerging as a key regulator of the mechanical
447 control of relaxation where stretch enhances LV relaxation during the transition from late
448 systole to early diastole(55, 58, 59) . In fact, Stehle et al. concluded that load-dependent
449 cross-bridge detachment is the only mechanism that explains how cardiac muscle can
450 relax as quickly as it contracts(60). Consistent with this, small stretches during the slow
451 phase of myofibril relaxation were shown to accelerate the onset of sarcomere “give”
452 which initiates the fast exponential phase of relaxation(61). We also recently showed that

453 loss of cMyBP-C significantly accelerates the fast phase of relaxation suggesting that
454 cMyBP-C provides an internal load (potentially by cross-linking thick and thin filaments) or
455 otherwise stabilizes sarcomere dynamics to slow relaxation(24).

456 In fast skeletal muscle acceleration of strain-dependent cross-bridge detachment after
457 loss of MyBP-C may contribute to the appearance of SA-like properties. For instance,
458 Wakefield et al. modeled cardiac tension transients in terms of a model where the shape
459 of the transient was the sum of 3 main factors: a passive Power-law relaxation term, a
460 Reversal term that is responsible for the transient drop in force ($P_2$ nadir), and a Drag term
461 that represents the initial fast rise in tension and relaxation immediately after the
462 stretch(59). If the Reversal term in skeletal muscle is small as suggested by Davis and
463 Epstein(32), and further limited by MyBP-C, then the shape of the tension transient in
464 skeletal muscle would be expected to be dominated by a combination of the Drag and
465 Power-law terms. However, if loss of fMyBP-C increases strain-dependent cross-bridge
466 detachment ($g_1$ in their model), then the Reversal term would become greater and deepen
467 the amplitude of the $P_2$ nadir(59). At the same time, loss of MyBP-C could further reduce
468 the Drag term as well as leading to an overall increase in the R/D ratio. Together, the two
469 effects would lead to the appearance of an SA response as observed following the loss of
470 fMyBP-C.

471 Through which interactions are the various MyBP-C isoforms able to affect the Drag and
472 Reversal terms? If MyBP-C links the thick and thin filaments and is able to slow filament
473 sliding(45, 57), then this interaction would be expected to increase the Drag term. MyBP-
474 C's presence may also limit the Reversal term, for instance, by preventing $P_i$-dependent
475 reversal of the powerstroke. Consistent with this cMyBP-C slows phosphate ($P_i$)-
476 dependent myosin cross-bridge detachment and prolongs cross-bridge lifetimes in cardiac

477 muscle (62, 63). Tanner et al. further concluded that cMyBP-C inhibits $P_i$-dependent
478 reversal of the powerstroke or otherwise stabilizes cross-bridge attachment in a way that
479 increases the probability of myosin completing its powerstroke(64). Notably, to account
480 for differences in relative rates of $P_2$ ($P_{2\text{-slow}}$) in different fiber types, Davis and Epstein
481 argued that $P_i$-dependent reversal of the powerstroke is largely absent in fast fibers,
482 whereas it is prominent in slow fibers(32). Straight et al. also concluded that a reverse
483 stroke of slow skeletal myosin accounts for augmentation of SA in slow skeletal muscle,
484 but not in fast skeletal muscle(34), although the same group later found that increases in
485 [$P_i$] concentration, such as during muscle fatigue, augments SA even in fast twitch
486 fibers(54). Using optical tweezers and synthetic cardiac myofilaments, Hwang et al.
487 demonstrated that a reversal stroke is present in cardiac myosin, but absent in fast skeletal
488 myosin, where it is a key determinant of cardiac contraction and relaxation and is further
489 necessary to produce stable force even at low levels of $Ca^{2+}$ activation(65). While the
490 reversal stroke (or absence of) is therefore likely intrinsic to the myosin isoform, our results
491 suggest that MyBP-C paralogs are key regulators of cross-bridge detachment rates,
492 potentially via modulation of $P_i$-dependent reversal of the powerstroke(66).

493 SA is a phenomenon best described in some insect flight muscles that operate at high
494 frequencies (100-1000 Hz) where muscle is turned on and off in response to mechanical
495 signals rather than being driven by slower and more energetically costly chemical and
496 electrical signals(35, 67, 68). In these so-called asynchronous muscles, a single action
497 potential elicits a sustained rise in [$Ca^{2+}$] that is permissive for multiple cycles of muscle
498 activation and relaxation driven by muscle stretch. The initiating mechanical event, muscle
499 stretch, itself is the result of contraction of an antagonistic muscle such that asynchronous
500 muscles act in pairs. By accelerating strain-induced cross-bridge detachment, it is

501 plausible that stretch synchronizes relaxation of a population of cross-bridges that contract
502 together resulting in SA. In this respect it is notable that MyBP-C, which appears to limit
503 strain-induced cross-bridge detachment as we show here, is absent in insect flight
504 muscles, although other proteins such as projectin and flightin may perform analogous
505 roles(69-71). While mammalian cardiac and skeletal muscles utilize a synchronous
506 contractile mechanism (where a single action potential leads to a single twitch), SA occurs
507 to some extent in both muscle types and may play important physiological roles. Examples
508 include coordinating proper ejection timing of the ventricle and mechanical control of
509 relaxation in the heart (55, 58, 72), or during exercise where contraction of one muscle
510 may lead to stretch in its antagonistic partner, priming it for contraction moments later(52,
511 54). Our results suggest that by modulating strain-dependent cross-bridge detachment
512 MyBP-C fine-tunes the contribution of SA in different muscle types and that regulation of
513 MyBP-C, for instance by phosphorylation within a given muscle type, may thus contribute
514 to a greater or lesser dependence on mechanical signals for activation and relaxation(33,
515 57).

516 **Potential mechanisms for MyBP-C regulation of the tension transient response**

517 To gain additional insights into mechanisms by which loss of MyBP-C affects cross-bridge
518 kinetics, we investigated structural effects of loss of MyBP-C using X-ray diffraction
519 analyses of $Ca^{2+}$-activated psoas muscle before and after cleavage of MyBP-C with TEVp.
520 We chose psoas muscle for X-ray diffraction studies because the effects of loss of MyBP-
521 C were greatest in psoas muscle (e.g., the reduction in $P_2$ was greatest) and because we
522 had previously characterized loss of MyBP-C in psoas muscle under relaxed
523 conditions(23). In that study we found that loss of MyBP-C expanded the sarcomere
524 lattice, reduced the length of the thin (actin) filament, and repositioned myosin heads from

525 their OFF to ON positions on the thick filament. These results were overall consistent with
526 effects of MyBP-C to stabilize the inhibited state of myosin and limit lattice expansion
527 potentially through interactions of MyBP-C with actin. By contrast, here we found under
528 $Ca^{2+}$-activated conditions that loss of MyBP-C did not significantly affect lattice spacing
529 possibly because strongly bound cross-bridges effectively limit the separation of the thick
530 and thin filaments. However, an indicator of lattice disorder or heterogeneity, $\sigma_D$, was
531 significantly increased at both SL 2.4 and SL 3.0 μm following loss of MyBP-C. Palmer et
532 al., also reported greater myofilament disorder in a mouse model of cMyBP-C
533 knockdown(63). $\sigma_D$ is increased during active conditions compared to passive conditions,
534 likely due to contributions of cross-bridge cycling that tend to move the positions of both
535 thick and thin filament relative to their equilibrium position in the lattice(73). Therefore,
536 results suggest that MyBP-C appears to plays a role in maintaining thick and thin filaments
537 near their equilibrium positions during contraction, possibly by linking thick and thin
538 filaments together. If so, then MyBP-C may promote efficient/strong cross-bridge binding
539 by maintaining alignment of binding sites relative to one another on thick and thin
540 filaments. Conversely, an increase in lattice disorder with loss of MyBP-C may lead to less
541 efficient binding of myosin cross-bridges and/or promote cross-bridge detachment,
542 thereby decreasing myosin duty ratio and increasing cycling rates(74, 75). The idea that
543 MyBP-C links thick and thin filaments together is also consistent with MyBP-C acting as a
544 drag force or internal load that slows cross-bridge cycling kinetics and relaxation(24, 45,
545 57).

546 MyBP-C also had significant effects on both the myosin head position and the thin filament.
547 The proportion of myosin heads in the ON state appeared unchanged following loss of
548 MyBP-C as indicated by the spacing of the M3 reflection ($S_{M3}$)(Supplementary Fig. X3),

549 but the ordering of the myosin heads relative to the thick filament backbone was
550 significantly decreased at both SLs as indicated by a reduction in the M3 intensity ($I_{M3}$)
551 (Fig. 6). Increased disorder of the myosin heads captured in the M3 intensity may be
552 indicative of less efficient cross-bridge binding to the thin filament and may explain the
553 faster cycling rates identified in mechanics experiments. Finally, loss of MyBP-C
554 decreased both the spacing of the third order troponin reflection ($S_{T3}$) and the spacing of
555 actin layer line 6 reflection ($S_{ALL6}$). The reduced spacing of these two actin-based
556 reflections indicate an overall reduction of thin filament length, consistent with the ability
557 of MyBP-C to bind to and exert a strain on the thin filament. In line with this, MyBP-C is
558 essential for thick filament stability and lattice rigidity(62, 63, 76). Notably, filament
559 compliance can affect stability of strongly bound cross-bridges and relaxation rates(77-
560 79). Taken together, the changes in X-ray diffraction reflections are consistent with a role
561 for MyBP-C in minimizing overall disorder of the sarcomere lattice during contraction and
562 maintaining myosin heads in ordered positions. Whereas proper alignment of thick and
563 thin filaments relative to one another may promote strong cross-bridge binding and cross-
564 bridge stability, loss of thick and thin filament alignment may promote cross-bridge
565 detachment, especially under strain.

566 **Limitations**

567 A limitation of our X-ray diffraction analysis was that structural changes were investigated
568 during isometric contraction, making it difficult to draw conclusions about whether dynamic
569 changes occur during rapid stretch that are not captured during steady state $Ca^{2+}$
570 activation. Future studies will include time-resolved X-ray diffraction measurements taken
571 as the muscle is being stretched in order to obtain structural information during the various
572 phases of the tension transient. Another limitation was that the soleus muscle contains a

573 mixed population of fast type and slow type fibers and we did not attempt to differentiate
574 their different contributions in mechanical force measurements. As a result, the
575 mechanical contribution of slow MyBP-C was likely underestimated due to the significant
576 presence of fast MyBP-C which was not subject to cleavage in $SpyC_1$ mice. In addition,
577 there are at least two splice variants of slow skeletal MyBP-C expressed in mouse and we
578 did not attempt to determine their relative expression(21).

579

580 **Conclusions**

581 Major conclusions from this study are that all 3 paralogs of MyBP-C (cardiac, fast skeletal
582 and slow skeletal) exert robust functional effects on force generation in their respective
583 muscle types. Using selective cleavage of each paralog we showed that all 3 had common
584 functional effects to increase $Ca^{2+}$ sensitivity of tension and limit cross-bridge cycling rates
585 at submaximal levels of activation. In addition, all 3 were effective at damping force
586 oscillations that appeared following loss of MyBP-C when MyBP-C was cleaved with
587 TEVp. Finally, all 3 paralogs slowed strain-dependent cross-bridge detachment rates
588 which was evident as accelerated detachment rates ($K_{rel}$) and a lower force nadir ($P_2$)
589 following loss of MyBP-C when muscles were subjected to a rapid stretch. However, the
590 overall transient force response to a rapid stretch was unique in each muscle type and
591 dependent on the MyBP-C paralog expressed. In particular, MyBP-C paralogs uniquely
592 modulated strain dependence of cross-bridge detachment and thereby influenced SA
593 properties in each muscle type. This regulation of cross-bridge relaxation may have
594 significant physiological importance, as strain-induced cross-bridge shortening is key to
595 rapid relaxation at onset of diastole to allow for proper ventricular filling, and may also
596 enable rapid bursts in contraction in skeletal muscle.

597
598
599 **Materials and Methods**
600
601 Animal procedures:

602 All animal procedures were performed under protocols approved by the Institutional
603 Animal Care and Use Committee (IACUC) at the University of Arizona. $SpyC_1$, $SnoopC_2$,
604 and $SpyC_3$ (C57BL6/NJ) mice were created by the Genetically Engineered Mouse Models
605 (GEMM) core at the University of Arizona. All mice were bred and housed in a pathogen-
606 free barrier animal facility at the University of Arizona. Animal genotypes were confirmed
607 using PCR of DNA extracted from toe-clip samples and amplicons visualized on 1%
608 agarose gels.

609

610 Mice used in this study were euthanized via cervical dislocation following anesthesia with
611 isoflurane. Left ventricles, psoas, and soleus muscles were immediately dissected and
612 flash frozen in liquid nitrogen for long-term storage at -80°C for force measurements. For
613 X-ray diffraction measurements, muscles were permeabilized using glyercol (1:1
614 rigor:glycerol where Rigor solution contained (in mM): KCl (100), $MgCl_2$ (2),
615 ethyleneglycol-bis(β-aminoethyl)-N,N,N',N'-tetraacetic acid (EGTA, 5), Tris (10),
616 dithiothreitol (DTT, 1), 1:100 HALT™ Protease Inhibitor Cocktail (ThermoFisher Scientific,
617 Waltham, MA, USA)) at 4°C for 48 hours. After 48 hours the solution was refreshed and
618 then muscles were stored up to 60 days at -20°C until use.

619

620 Recombinant protein expression and purification:

621 Protein plasmids with desired DNA sequences were purchased from Genscript
622 (Piscataway, NJ, USA). BL21 and DE3 competent cells (C2527, New England Biolabs,
623 Ipswich, MA, USA) were transfected with plasmid DNA and protein purification was
624 performed as described previously.(13, 22)

625

626 Muscle force measurements:

627 Tissue was thawed in a skinning solution consisting of a Relax Buffer containing 1% Triton
628 X-100, 0.1% Saponin, and 1:100 HALT™ Protease Inhibitor Cocktail (ThermoFisher
629 Scientific, Waltham, MA, USA). Relax buffer contained (in mM): 100 KCl, 10 imidazole, 2
630 EGTA, 5 $MgCl_2$, 4 ATP (A2383, Sigma, St. Louis, MO, USA), and 1:100 HALT™ Protease
631 Inhibitor Cocktail at pH of 7.0. Multicellular preparations of cardiac cells and skeletal
632 muscle fibers were then isolated by mechanical disruption using a homogenizer (Omni
633 International 60CE54. Model: TH115). After homogenization, cardiac and skeletal muscle
634 cells were incubated with rotation in a skinning solution at 4°C for 15 and 30 min,
635 respectively. Detergent-permeabilized cardiac and skeletal muscle cells were then
636 washed thoroughly with fresh Relax buffer to remove residual detergents. Next, cardiac
637 cells and skeletal muscle fibers (~80-200 mm in length, 50-100 mm in width) were selected
638 and attached to a high-speed positional motor (Model: 315C-I, Aurora Scientific Inc.,
639 Aurora, Ontario, Canada) and a force transducer (Model 403 A series, Aurora Scientific
640 Inc., Aurora, Ontario, Canada) using aquarium sealant (Marineland, 100% clear silicone
641 rubber or Loctite, Clear Silicone Waterproof Multipurpose Adhesive Sealant). The
642 positional motor and force transducer were attached over a temperature-adjustable 8-well
643 platform (Model 803B, Aurora Scientific Inc., Aurora, Ontario, Canada) regulated by a
644 thermocouple (825A, Aurora Scientific Inc., Aurora, ON, Canada). The 8-well platform was

645 then mounted on the stage of an inverted light microscope (Model IX-53, Olympus
646 Instrument Co., Japan). The aquarium sealant was allowed to cure for 30 min before the
647 experiment was started. SL was then measured using video imaging in passive conditions
648 (at pCa 9.0) and SL was set to a final length of 2.3 μm and 2.4 μm for cardiac and skeletal
649 muscle, respectively. All muscle force measurements were obtained at 15°C using a range
650 of pCa solutions with free $Ca^{2+}$ pCa 9.0 to 4.5, where pCa = -log[$Ca^{2+}$]. Force
651 measurements (F) recorded at each submaximal pCa solution were normalized to the
652 maximal force ($F_0$) at pCa 4.5 and to cross-sectional area of the muscle fiber assuming
653 circular dimensions. Data was fitted using a sigmoidal four-parameter logistic curve within
654 Graphpad Prism. $k_{tr}$ was assessed by performing a slack-restretch test, where the muscle
655 was shortened to 80% of its reference length for 20 ms, stretched to 105% reference
656 length for 5 ms and returned to reference length. Tension transient parameters were
657 assessed by performing a rapid 2% stretch over 5 ms and held for 3 s. Cross-bridge
658 cycling rates ($k_{tr}$ and shortening induced $k_{df}$) and cross-bridge relaxation ($k_{rel}$), were fit
659 using a single exponential curve and normalized to maximal rate ($k_0$) at pCa 4.5 and
660 plotted against isometric force.

661

662 N-terminal MyBP-C cleavage and *in situ* paste of recombinant proteins:

663 Mechanics experiments typically consisted of 3 consecutive sets of measurements: First,
664 before N-terminal cleavage of MyBP-C (control), second, after N-terminal cleavage of
665 MyBP-C with TEVp, and third in a subset of experiments after *in situ* paste of recombinant
666 MyBP-C. Proteolytic cleavage of domains C0-C7 in cardiac cells and C1-C7 in skeletal
667 muscle cells was performed by incubating myocytes in 20 μM AcTEV™ Protease

668 (ThermoFisher, 12575015) at 25°C for 30 min while the permeabilized muscle preparation
669 was attached to the high-speed positional motor and force transducer. After TEVp
670 incubation, cells were rigorously washed in fresh relax buffer (3 x for 3 min) to remove
671 TEV protease as well as cleaved endogenous MyBP-C N-terminal domains. Paste of
672 recombinant protein was done by incubating permeabilized cell preparations for 15 min at
673 15°C with 20 μM recombinant protein of choice containing a SpyCatcher sequence.
674 Myocytes were then washed (3 x for 3 min) using fresh relax buffer to remove excess
675 (non-ligated) recombinant protein. N-terminal MyBP-C cleavage and protein ligation was
676 assessed using SDS-PAGE gel electrophoresis and western blot as described
677 previously(23).

678 Small angle X-ray diffraction:

679 All X-ray diffraction experiments were performed with the small-angle instrument at the
680 BioCAT beamline 18ID at the Advanced Photon Source, Argonne National Laboratory.
681 Muscle experiments were performed both before and after the facility wide upgrade of
682 the Advanced Photon Source with changes to beam flux (Pre: ~$3x10^{12}$, Post: ~$5x10^{13}$
683 photons per second). The X-ray diffraction beam (0.103 nm wavelength), focusing at the
684 detector plane (Pre: ~0.06 x 0.15 mm. Post: 0.02 x 0.02 mm), sample to detector
685 distance (~2m), and detector (Mar 165, Rayonix Inc., USA) are identical to our previous
686 study in relaxed muscle fibers(23). An in-line camera was present to properly target
687 beam onto muscle fibers and assess for any irregularities in attachment of the muscle.
688 Muscle fibers were attached to custom fabricated clamps and connected to a high-speed
689 length controller (322C, Aurora Scientific, Canada) and a force transducer (402A, Aurora
690 Scientific, Canada) with a sampling rate of 1,000 Hz. Measurements from the force
691 transducer to identify activation levels of the fibers were visualized using Real Time

692 Muscle Data Acquisition and Analysis system (600A, Aurora Scientific, Canada).
693 Experiments were performed at ~25°C. SL was set at SL 2.4 μm or SL 3.0 μm using a 4-
694 mW Helium-Neon laser based on width of the first-order diffraction. Muscles were
695 activated by removal of relaxing solution (in mM: potassium propionate (45.3), N,N-
696 Bis(2-hydroxyethyl)-2-aminoethanesulfonic acid BES (40); EGTA (10), $MgCl_2$ (6.3), Na-
697 ATP (6.1), DTT (10), protease inhibitors [Complete], pH 7.0), three 30 second
698 incubations with pre-activating solution (in mM: potassium propionate (45.3), N,N-Bis(2-
699 hydroxyethyl)-2-aminoethanesulfonic acid BES (40); $MgCl_2$ (6.3), Na-ATP (6.1), DTT
700 (10), protease inhibitors [Complete], pH 7.0), and finally by incubation with pCa 6.0
701 solution (in mM: potassium propionate (170), magnesium acetate (2.5), MOPS (10) and
702 ATP (2.5), and CaEGTA and $K_2$EGTA were mixed at different proportions to obtain
703 different pCa ($-\log[Ca^{2+}]$), pH 7.0) values. Following incubation with pCa 6.0, tension
704 was monitored until the muscle reached a steady-state level of force, upon which the
705 bath was lowered with a servo-motor and X-ray images were taken in open air. No part
706 of the sample was exposed to the X-ray beam more than once. Samples then underwent
707 TEVp protease incubation as described above, and the process was repeated.

708 X-ray Diffraction Analysis:

709 Analysis of x-ray diffraction patterns was performed using MuscleX (version 1.22.0)
710 open-source data reduction and analysis package (BioCAT, Argonne National
711 Laboratories) as previously described(23, 80).

712 Statistics:

713 Statistical analyses were performed either in Graphpad Prism or JMP Pro (V16, SAS
714 Institute Inc., Cary, NC, USA). All measurements reported as the mean ± SEM.

715 Repeated measures one-way ANOVA tests with main effects pCa, TEVp treatment, and
716 their interaction, as well as an individual fiber random effect were performed on
717 measurements before TEV protease cleavage, after TEV protease cleavage, and when
718 present, after addition of recombinant protein. A mixed effects test was used for any
719 missing values. A paired t-test was used specifically to compare pCa50 values. The
720 significance level was $p<0.05$.

721
722 **Acknowledgments**
723
724 This research was performed on APS beam time award(s) from the Advanced Photon
725 Source, a U.S. Department of Energy (DOE) Office of Science user facility operated for
726 the DOE Office of Science by Argonne National Laboratory under Contract No. DE-
727 AC02-06CH11357. BioCAT is supported by grant P30 GM138395 from the National
728 Institute of General Medical Sciences of the National Institutes of Health. The content is
729 solely the responsibility of the authors and does not necessarily reflect the official views
730 of the National Institute of General Medical Sciences or the National Institutes of Health.
731 We would like to thank Dr. Thomas C Irving for expertise and help with editing the
732 manuscript and John Sullivan for generating a video of SPOC in soleus muscle. Funding
733 for this study was provided by the National Institute of Health (HL080367 [SPH]),
734 HL140925 [SPH], AR081935 [SPH], T32 HL007249 [NME]), the American Heart
735 Association (827628 [NME]), and German Research Foundation (DFG) 454867250 to
736 ALH.
737
738 **References**
739
740

741 1. L. Heling, M. A. Geeves, N. M. Kad, MyBP-C: one protein to govern them all. *J Muscle Res*
742 *Cell Motil* **41**, 91–101 (2020).
743 2. D. Tamborrini *et al.*, Structure of the native myosin filament in the relaxed cardiac
744 sarcomere. *Nature* **623**, 863–871 (2023).
745 3. D. Dutta, V. Nguyen, K. S. Campbell, R. Padron, R. Craig, Cryo-EM structure of the human
746 cardiac myosin filament. *Nature* **623**, 853–862 (2023).
747 4. M. V. Razumova, K. L. Bezold, A. Y. Tu, M. Regnier, S. P. Harris, Contribution of the
748 myosin binding protein C motif to functional effects in permeabilized rat trabeculae. *J*
749 *Gen Physiol* **132**, 575–585 (2008).
750 5. A. E. Whitten, C. M. Jeffries, S. P. Harris, J. Trewhella, Cardiac myosin-binding protein C
751 decorates F-actin: implications for cardiac function. *Proc Natl Acad Sci U S A* **105**, 18360–
752 18365 (2008).
753 6. G. Kunst *et al.*, Myosin binding protein C, a phosphorylation-dependent force regulator
754 in muscle that controls the attachment of myosin heads by its interaction with myosin
755 S2. *Circ Res* **86**, 51–58 (2000).

756 7. A. Ababou, M. Gautel, M. Pfuhl, Dissecting the N-terminal myosin binding site of human
757 cardiac myosin-binding protein C. Structure and myosin binding of domain C2. *J Biol*
758 *Chem* **282**, 9204–9215 (2007).
759 8. C. Risi *et al.*, N-Terminal Domains of Cardiac Myosin Binding Protein C Cooperatively
760 Activate the Thin Filament. *Structure* **26**, 1604–1611 e1604 (2018).
761 9. J. Y. Mun *et al.*, Myosin-binding protein C displaces tropomyosin to activate cardiac thin
762 filaments and governs their speed by an independent mechanism. *Proc Natl Acad Sci U S*
763 *A* **111**, 2170–2175 (2014).
764 10. S. Nelson, S. Beck-Previs, S. Sadayappan, C. Tong, D. M. Warshaw, Myosin-binding
765 protein C stabilizes, but is not the sole determinant of SRX myosin in cardiac muscle. *J*
766 *Gen Physiol* **155** (2023).
767 11. J. W. McNamara *et al.*, Ablation of cardiac myosin binding protein-C disrupts the super-
768 relaxed state of myosin in murine cardiomyocytes. *J Mol Cell Cardiol* **94**, 65–71 (2016).
769 12. C. Y. Doh *et al.*, Molecular characterization of linker and loop-mediated structural
770 modulation and hinge motion in the C4-C5 domains of cMyBPC. *J Struct Biol* **214**,
771 107856 (2022).
772 13. A. C. Greenman, R. L. Sadler, S. P. Harris, Autoinhibition of cMyBP-C by its middle
773 domains. *J Mol Cell Cardiol* **200**, 82–92 (2025).
774 14. A. A. Glazier, A. Thompson, S. M. Day, Allelic imbalance and haploinsufficiency in
775 MYBPC3-linked hypertrophic cardiomyopathy. *Pflugers Arch* **471**, 781–793 (2019).
776 15. S. P. Harris, R. G. Lyons, K. L. Bezold, In the thick of it: HCM-causing mutations in myosin
777 binding proteins of the thick filament. *Circ Res* **108**, 751–764 (2011).
778 16. A. S. Helms *et al.*, Spatial and Functional Distribution of MYBPC3 Pathogenic Variants
779 and Clinical Outcomes in Patients With Hypertrophic Cardiomyopathy. *Circ Genom*
780 *Precis Med* **13**, 396–405 (2020).
781 17. C. A. Gurnett *et al.*, Myosin binding protein C1: a novel gene for autosomal dominant
782 distal arthrogryposis type 1. *Hum Mol Genet* **19**, 1165–1173 (2010).
783 18. J. W. McNamara, S. Sadayappan, Skeletal myosin binding protein-C: An increasingly
784 important regulator of striated muscle physiology. *Arch Biochem Biophys* **660**, 121–128
785 (2018).
786 19. J. M. Mariano *et al.*, Pulsatile Myofilament Activity in Myotrem Myopathy Associated
787 with Myogenic Tremor. *Int J Mol Sci* **26** (2025).
788 20. C. E. Oakley, B. D. Hambly, P. M. Curmi, L. J. Brown, Myosin binding protein C: structural
789 abnormalities in familial hypertrophic cardiomyopathy. *Cell Res* **14**, 95–110 (2004).
790 21. M. A. Ackermann, A. Kontrogianni-Konstantopoulos, Myosin binding protein-C slow: a
791 multifaceted family of proteins with a complex expression profile in fast and slow twitch
792 skeletal muscles. *Front Physiol* **4**, 391 (2013).
793 22. N. C. Napierski *et al.*, A Novel "Cut and Paste" Method for In Situ Replacement of
794 cMyBP-C Reveals a New Role for cMyBP-C in the Regulation of Contractile Oscillations.
795 *Circ Res* **126**, 737–749 (2020).
796 23. A. L. Hessel *et al.*, Myosin-binding protein C regulates the sarcomere lattice and
797 stabilizes the OFF states of myosin heads. *Nat Commun* **15**, 2628 (2024).
798 24. A. V. Dvornikov, S. P. Harris, Myosin-binding protein C slows cardiac myofibril relaxation
799 kinetics. *J Physiol* **603**, 5351–5368 (2025).
800 25. B. Zakeri *et al.*, Peptide tag forming a rapid covalent bond to a protein, through
801 engineering a bacterial adhesin. *Proc Natl Acad Sci U S A* **109**, E690–697 (2012).

802 26. G. Veggiani *et al.*, Programmable polyproteams built using twin peptide superglues. *Proc*
803 *Natl Acad Sci U S A* **113**, 1202–1207 (2016).
804 27. B. Brenner, E. Eisenberg, Rate of force generation in muscle: correlation with
805 actomyosin ATPase activity in solution. *Proc Natl Acad Sci U S A* **83**, 3542–3546 (1986).
806 28. G. K. Dhoot, M. C. Hales, B. M. Grail, S. V. Perry, The isoforms of C protein and their
807 distribution in mammalian skeletal muscle. *J Muscle Res Cell Motil* **6**, 487–505 (1985).
808 29. J. E. Wolfe *et al.*, SPontaneous Oscillatory Contraction (SPOC): auto-oscillations observed
809 in striated muscle at partial activation. *Biophys Rev* **3**, 53–62 (2011).
810 30. A. F. Huxley, R. M. Simmons, Proposed mechanism of force generation in striated
811 muscle. *Nature* **233**, 533–538 (1971).
812 31. L. E. Ford, A. F. Huxley, R. M. Simmons, Tension responses to sudden length change in
813 stimulated frog muscle fibres near slack length. *J Physiol* **269**, 441–515 (1977).
814 32. J. S. Davis, N. D. Epstein, Kinetic effects of fiber type on the two subcomponents of the
815 Huxley-Simmons phase 2 in muscle. *Biophys J* **85**, 390–401 (2003).
816 33. J. E. Stelzer, R. L. Moss, Contributions of stretch activation to length-dependent
817 contraction in murine myocardium. *J Gen Physiol* **128**, 461–471 (2006).
818 34. C. R. Straight, K. M. Bell, J. N. Slosberg, M. S. Miller, D. M. Swank, A myosin-based
819 mechanism for stretch activation and its possible role revealed by varying phosphate
820 concentration in fast and slow mouse skeletal muscle fibers. *Am J Physiol Cell Physiol*
821 **317**, C1143–C1152 (2019).
822 35. M. Linari, M. K. Reedy, M. C. Reedy, V. Lombardi, G. Piazzesi, Ca-activation and stretch-
823 activation in insect flight muscle. *Biophys J* **87**, 1101–1111 (2004).
824 36. J. O. Vigoreaux, J. Vigoreaux, SpringerLink (2006) Nature's versatile engine : insect flight
825 muscle inside and out. in *Molecular Biology Intelligence Unit* (Landes
826 Bioscience/Eurekah.com

827 Springer Science+Business Media

828 Springer US, Georgetown, Tex

829 New York, N.Y

830 New York, NY).
831 37. R. Rice *et al.*, Cardiac myosin heavy chain isoform exchange alters the phenotype of
832 cTnT-related cardiomyopathies in mouse hearts. *J Mol Cell Cardiol* **48**, 979–988 (2010).
833 38. B. C. Tanner, Y. Wang, J. Robbins, B. M. Palmer, Kinetics of cardiac myosin isoforms in
834 mouse myocardium are affected differently by presence of myosin binding protein-C. *J*
835 *Muscle Res Cell Motil* **35**, 267–278 (2014).
836 39. R. Mamidi, K. S. Gresham, S. Verma, J. E. Stelzer, Cardiac Myosin Binding Protein-C
837 Phosphorylation Modulates Myofilament Length-Dependent Activation. *Front Physiol* **7**,
838 38 (2016).
839 40. W. Ma, T. C. Irving, Small Angle X-ray Diffraction as a Tool for Structural Characterization
840 of Muscle Disease. *Int J Mol Sci* **23** (2022).
841 41. A. L. Hessel *et al.*, The distinctive mechanical and structural signatures of residual force
842 enhancement in myofibers. *Proc Natl Acad Sci U S A* **121**, e2413883121 (2024).
843 42. V. Joumaa *et al.*, Effect of Active Lengthening and Shortening on Small-Angle X-ray
844 Reflections in Skinned Skeletal Muscle Fibres. *Int J Mol Sci* **22** (2021).

845 43. G. Piazzesi *et al.*, Changes in conformation of myosin heads during the development of
846 isometric contraction and rapid shortening in single frog muscle fibres. *J Physiol* **514 ( Pt**
847 **2)**, 305–312 (1999).
848 44. H. E. Huxley, W. Brown, The low-angle x-ray diagram of vertebrate striated muscle and
849 its behaviour during contraction and rigor. *J Mol Biol* **30**, 383–434 (1967).
850 45. F. S. Korte, K. S. McDonald, S. P. Harris, R. L. Moss, Loaded shortening, power output,
851 and rate of force redevelopment are increased with knockout of cardiac myosin binding
852 protein-C. *Circ Res* **93**, 752–758 (2003).
853 46. T. Song *et al.*, Fast skeletal myosin-binding protein-C regulates fast skeletal muscle
854 contraction. *Proc Natl Acad Sci U S A* **118** (2021).
855 47. K. Sato, M. Ohtaki, Y. Shimamoto, S. Ishiwata, A theory on auto-oscillation and
856 contraction in striated muscle. *Prog Biophys Mol Biol* **105**, 199–207 (2011).
857 48. T. Kagemoto, A. Li, C. Dos Remedios, S. Ishiwata, Spontaneous oscillatory contraction
858 (SPOC) in cardiomyocytes. *Biophys Rev* **7**, 15–24 (2015).
859 49. X. Li *et al.*, Two novel mutations in myosin binding protein C slow causing distal
860 arthrogryposis type 2 in two large Han Chinese families may suggest important
861 functional role of immunoglobulin domain C2. *PLoS One* **10**, e0117158 (2015).
862 50. K. Ha *et al.*, MYBPC1 mutations impair skeletal muscle function in zebrafish models of
863 arthrogryposis. *Hum Mol Genet* **22**, 4967–4977 (2013).
864 51. S. P. Harris, Making waves: A proposed new role for myosin-binding protein C in
865 regulating oscillatory contractions in vertebrate striated muscle. *J Gen Physiol* **153**
866 (2021).
867 52. J. C. Robinett, L. M. Hanft, B. Biesiadecki, K. S. McDonald, Molecular regulation of
868 stretch activation. *Am J Physiol Cell Physiol* **323**, C1728–C1739 (2022).
869 53. S. Galler, O. Andruchov, G. M. Stephenson, D. G. Stephenson, Qualitatively different
870 cross-bridge attachments in fast and slow muscle fiber types. *Biochem Biophys Res*
871 *Commun* **385**, 44–48 (2009).
872 54. P. C. Woods, D. M. Swank, M. S. Miller, Stretch activation combats force loss from
873 fatigue in fast-contracting mouse skeletal muscle fibers. *J Gen Physiol* **157** (2025).
874 55. B. M. Palmer *et al.*, Enhancing diastolic function by strain-dependent detachment of
875 cardiac myosin crossbridges. *J Gen Physiol* **152** (2020).
876 56. R. H. Abbott, G. J. Steiger, Temperature and amplitude dependence of tension transients
877 in glycerinated skeletal and insect fibrillar muscle. *J Physiol* **266**, 13–42 (1977).
878 57. J. C. Robinett, L. M. Hanft, J. Geist, A. Kontrogianni-Konstantopoulos, K. S. McDonald,
879 Regulation of myofilament force and loaded shortening by skeletal myosin binding
880 protein C. *J Gen Physiol* **151**, 645–659 (2019).
881 58. C. S. Chung, C. W. Hoopes, K. S. Campbell, Myocardial relaxation is accelerated by fast
882 stretch, not reduced afterload. *J Mol Cell Cardiol* **103**, 65–73 (2017).
883 59. J. I. Wakefield, S. P. Bell, B. M. Palmer, Inorganic phosphate accelerates cardiac
884 myofilament relaxation in response to lengthening. *Front Physiol* **13**, 980662 (2022).
885 60. R. Stehle *et al.*, Mechanical properties of sarcomeres during cardiac myofibrillar
886 relaxation: stretch-induced cross-bridge detachment contributes to early diastolic filling.
887 *J Muscle Res Cell Motil* **27**, 423–434 (2006).
888 61. C. Poggesi, C. Tesi, R. Stehle, Sarcomeric determinants of striated muscle relaxation
889 kinetics. *Pflugers Arch* **449**, 505–517 (2005).

890 62. B. M. Palmer *et al.*, Effect of cardiac myosin binding protein-C on mechanoenergetics in
891 mouse myocardium. *Circ Res* **94**, 1615–1622 (2004).
892 63. B. M. Palmer *et al.*, Roles for cardiac MyBP-C in maintaining myofilament lattice rigidity
893 and prolonging myosin cross-bridge lifetime. *Biophys J* **101**, 1661–1669 (2011).
894 64. B. C. W. Tanner, M. J. Previs, Y. Wang, J. Robbins, B. M. Palmer, Cardiac myosin binding
895 protein-C phosphorylation accelerates beta-cardiac myosin detachment rate in mouse
896 myocardium. *Am J Physiol Heart Circ Physiol* **320**, H1822–H1835 (2021).
897 65. Y. Hwang, T. Washio, T. Hisada, H. Higuchi, M. Kaya, A reverse stroke characterizes the
898 force generation of cardiac myofilaments, leading to an understanding of heart function.
899 *Proc Natl Acad Sci U S A* **118** (2021).
900 66. M. S. Woody, D. A. Winkelmann, M. Capitanio, E. M. Ostap, Y. E. Goldman, Single
901 molecule mechanics resolves the earliest events in force generation by cardiac myosin.
902 *Elife* **8** (2019).
903 67. J. W. Pringle, The excitation and contraction of the flight muscles of insects. *J Physiol*
904 **108**, 226–232 (1949).
905 68. G. J. Steiger, J. C. Ruegg, Energetics and "efficiency" in the isolated contractile machinery
906 of an insect fibrillar muscle at various frequencies of oscillation. *Pflugers Arch* **307**, 1–21
907 (1969).
908 69. T. P. Vu Manh *et al.*, Expression of cardiac myosin-binding protein-C (cMyBP-C) in
909 Drosophila as a model for the study of human cardiomyopathies. *Hum Mol Genet* **14**, 7–
910 17 (2005).
911 70. M. C. Reedy, B. Bullard, J. O. Vigoreaux, Flightin is essential for thick filament assembly
912 and sarcomere stability in Drosophila flight muscles. *J Cell Biol* **151**, 1483–1500 (2000).
913 71. B. Bullard, A. Pastore, Through thick and thin: dual regulation of insect flight muscle and
914 cardiac muscle compared. *J Muscle Res Cell Motil* **40**, 99–110 (2019).
915 72. K. B. Campbell, M. Chandra, Functions of stretch activation in heart muscle. *J Gen*
916 *Physiol* **127**, 89–94 (2006).
917 73. L. C. Yu, A. C. Steven, G. R. Naylor, R. C. Gamble, R. J. Podolsky, Distribution of mass in
918 relaxed frog skeletal muscle and its redistribution upon activation. *Biophys J* **47**, 311–
919 321 (1985).
920 74. T. L. Daniel, A. C. Trimble, P. B. Chase, Compliant realignment of binding sites in muscle:
921 transient behavior and mechanical tuning. *Biophys J* **74**, 1611–1621 (1998).
922 75. I. A. Telley, J. Denoth, E. Stussi, G. Pfitzer, R. Stehle, Half-sarcomere dynamics in
923 myofibrils during activation and relaxation studied by tracking fluorescent markers.
924 *Biophys J* **90**, 514–530 (2006).
925 76. L. R. Nyland *et al.*, Cardiac myosin binding protein-C is essential for thick-filament
926 stability and flexural rigidity. *Biophys J* **96**, 3273–3280 (2009).
927 77. K. S. Campbell, Filament compliance effects can explain tension overshoots during force
928 development. *Biophys J* **91**, 4102–4109 (2006).
929 78. B. Kiss *et al.*, Nebulin stiffens the thin filament and augments cross-bridge interaction in
930 skeletal muscle. *Proc Natl Acad Sci U S A* **115**, 10369–10374 (2018).
931 79. K. S. Campbell, Compliance Accelerates Relaxation in Muscle by Allowing Myosin Heads
932 to Move Relative to Actin. *Biophys J* **110**, 661–668 (2016).
933 80. J. Jiratrakanvong *et al.*, MuscleX: data analysis software for fiber diffraction patterns
934 from muscle. *J Synchrotron Radiat* **31**, 1401–1408 (2024).

935

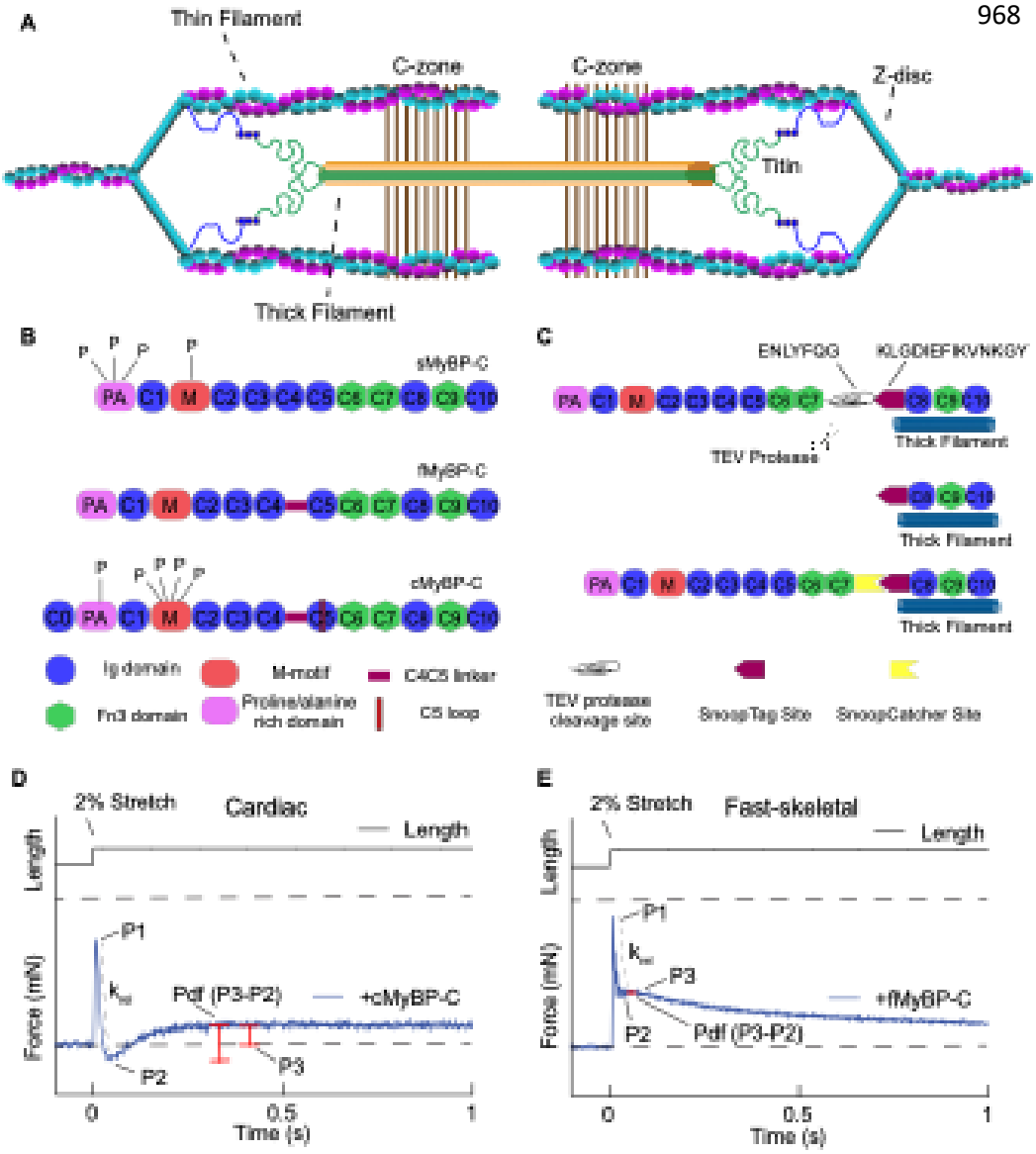


**Figure 1:** Sarcomere organization, MyBP-C structure, and utilization of the "cut-and-paste" mouse models to investigate muscle response to rapid stretch. A) Illustration of a muscle sarcomere highlighting Myosin Binding Protein-C location in the C-zone. B) Schematic of slow, fast skeletal, and cardiac Myosin Binding Protein-C paralogs. Slow and cardiac isoforms contain variable phosphorylation sites within the proline/alanine-rich as well as M-domain. Both fast and cardiac contain a linker between domains C4C5 while slow does not. Cardiac MyBP-C also contains an additional N-terminal immunoglobulin domain termed C0 as well as a 28 amino acid loop within the C5 domain. C) Schematic representation of the cut-and-paste system in fast skeletal Myosin Binding Protein-C. D) Representative force transient traces from cardiac and skeletal muscle highlighting shape differences and defining stretch activation terms for different muscle type.

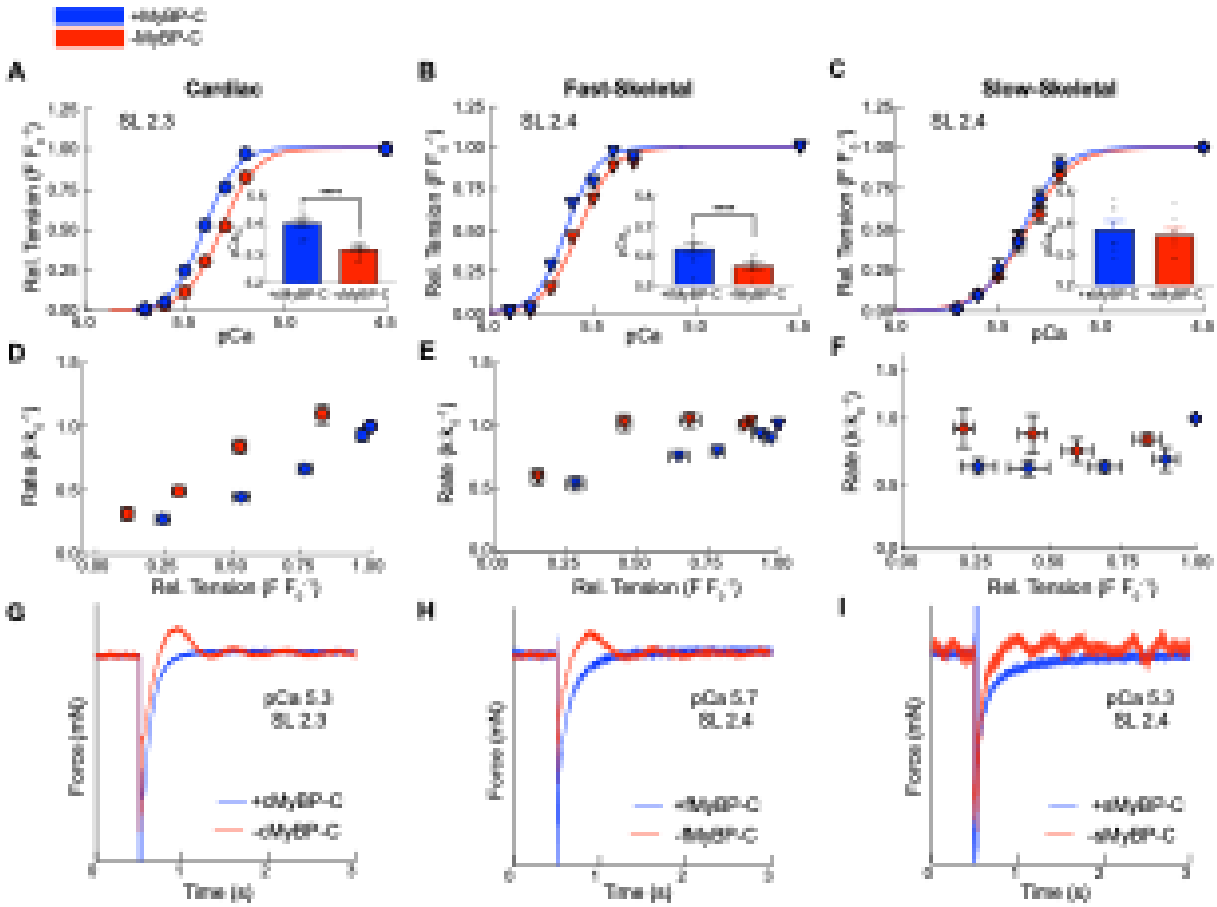


**Figure 2:** Removal of MyBP-C alters $Ca^{2+}$-sensitivity, cross-bridge cycling rates, and produces oscillatory contractions in each muscle type. A-C) Tension-pCa curves for cardiac (A), fast skeletal (B), and slow skeletal (C) before (blue) and after (red) removal of MyBP-C. D-F) Changes in cross-bridge cycling rates in cardiac (D), fast (E), and slow skeletal (F) before and after removal of MyBP-C. G-I) Representative force traces highlighting force overshoots and tension oscillations at steady-state force in cardiac (G), fast (H), and slow skeletal (I) before and after removal of MyBP-C. Force traces only in Figure 3i (sMyBP-C) were smoothed for clearer visualization of oscillations on Graphpad Prism. Data presented as mean ± s.e.m. $pCa_{50}$ values assessed with paired t-test. **** = $p < 0.0001$ in (a-c). $k_{tr}$ assessed with a two-way ANOVA with pCa and treatment as main effects also assessing their interaction. Individual fiber was included as a random effect. Treatment showed significance in (D-F) (D: Treatment: Prob > F = 0.0254, E: Treatment*pCa Prob > F = < 0.0033, F: Treatment Prob > F = 0.0038) A Student's t-test or Tukey Honestly Statistically Different (HSD) post-hoc test was performed on significant main effects ($p < 0.05$). Dataset from: Cardiac (n=13 cardiomyocytes. N=4 mice). Psoas (n=10 fibers. N=3 mice). Soleus (n=8. N=3 +sMyBP-C. N=4 -sMyBP-C). Figure 2B, 2E, and 2H appear in Hessel et, al. 2024 publication in Nature Communications. (23).

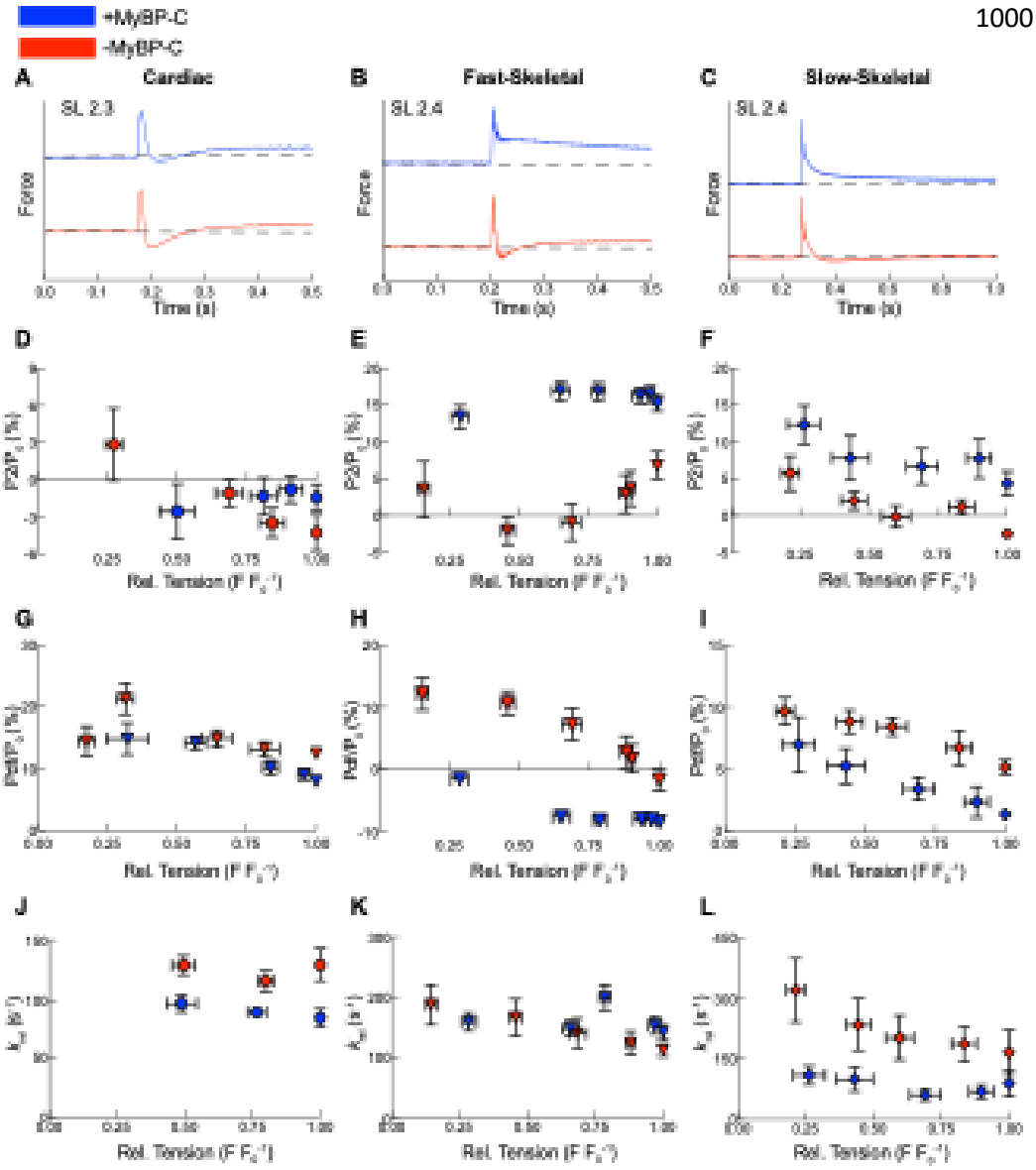


**Figure 3**: MyBP-C paralogs differentially affect tension transients following rapid stretch in each muscle type **a-c:** Representative force traces following 2% rapid stretch before (blue) and after (red)TEVp treatment of cardiac (a) fast skeletal psoas (b), and slow skeletal soleus (c). **d-f:** Mechanical measurements of the $P_2$ nadir before and after TEVp treatment in cardiac (d)(pCa*Treatment Prob > F = <0.0001, fast skeletal psoas (e) (Treatment Prob > F = <0.0001, and slow skeletal soleus (f) (n.s). **g-i:** Mechanical measurements of $P_{df}$, the amplitude of delayed force redevelopment, before and after TEVp treatment of cardiac (g)(Treatment Prob > F = 0.0001), fast skeletal psoas (h)(Treatment*pCa Prob > F = 0.0118), and slow skeletal soleus (i)(Treatment Prob > F = 0.006). **j-l:** Mechanical measurements of the rate of cross-bridge relaxation ($k_{rel}$) following rapid 2% stretch before and after TEVp treatment of cardiac (j)(Prob > F = <0.0001), fast skeletal psoas (k)(Treatment: Prob > F = 0.0272), and slow skeletal soleus (l)(n.s). Data presented as mean ± s.e.m. A repeated measures ANOVA design was performed

1013 throughout with pCa, treatment, and their interaction as main effects. A random effect was
1014 included for each individual fiber. A Student's t-test or Tukey's HSD post-hoc test was performed
1015 on significant main effects ($p < 0.05$). Dataset: Cardiac from (n=13 cardiomyocytes. N=4 mice).
1016 Psoas (n=10 fibers. N=3 mice). Soleus (n=8. N=3 +sMyBP-C. N=4 -sMyBP-C). Further detail in
1017 supplement.

1018

1019

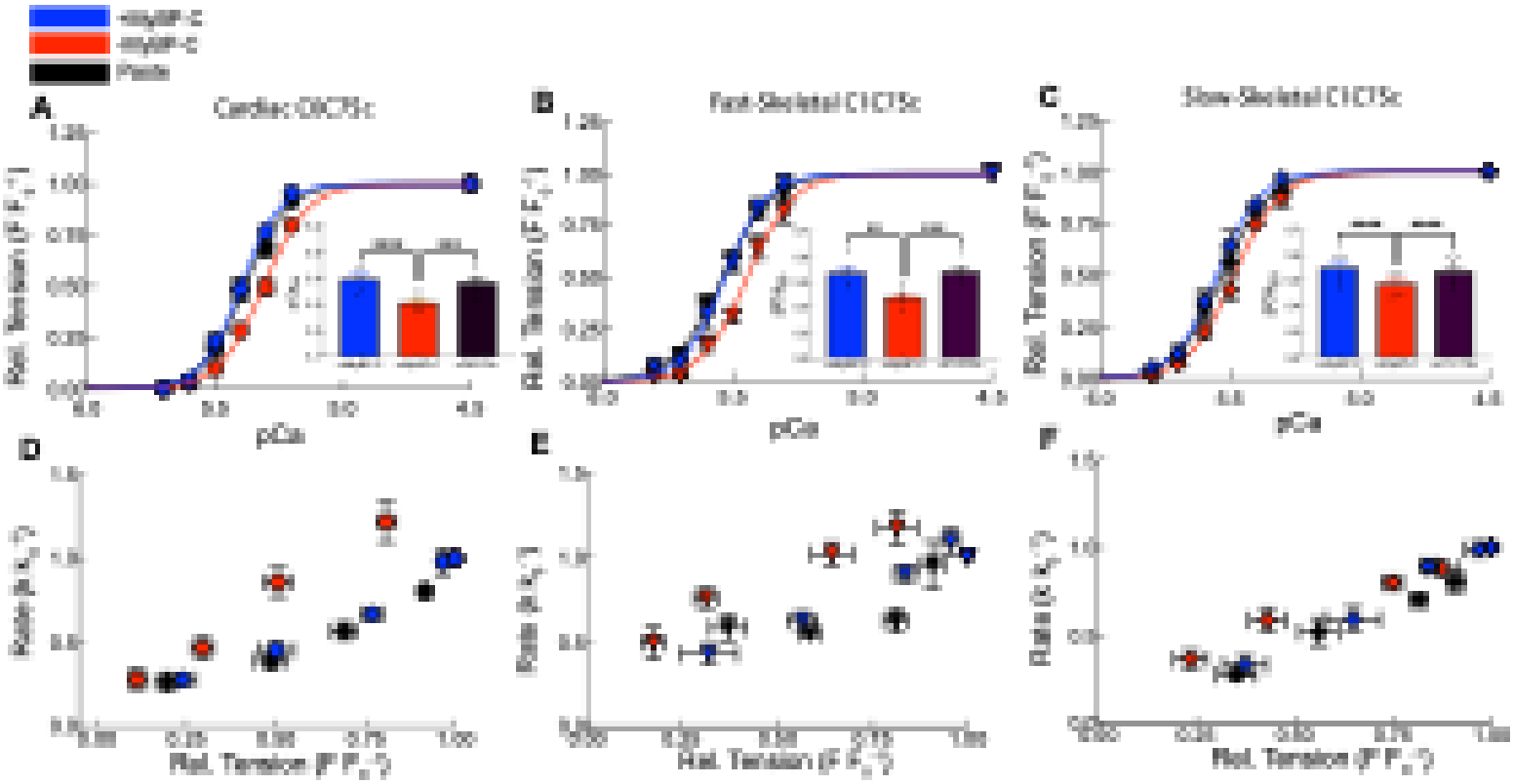


**Figure 4:** Cut-and-paste experiments performed in detergent permeabilized cardiac muscle to assess $Ca^{2+}$-sensitivity and $k_{tr}$ after *in situ* replacement of recombinant cardiac, fast skeletal, and slow skeletal MyBP-C. **a-c:** Relative tension-pCa with inset containing average $pCa_{50}$ following each curve for cC0C7Sc(a), fC1C7Sc (b), and sC1C7Sc (c). ** = p = <0.0001, *** p < 0.0005, **** p = <0.005 **d-f:** Changes in $k_{tr}$ before and after removal of endogenous cMyBP-C and following paste of cC0C7Sc (d) (pCa*Treatment Prob > F = 0.0046), fC1C7Sc (e) (Treatment Prob > F = 0.0061) and sC1C7Sc (f) (Treatment Prob > F = 0.0046). Statistics throughout are an ANOVA design with pCa, treatment, and their interaction as main effects, as well as an individual fiber random effect. Statistically significant differences were assessed using a Tukey's HSD post-hoc test on statistically significant differences (p < 0.05). Dataset: cC0C7Sc (n=7, N=3), fC1C7Sc (n=6, N=5), sC1C7Sc (n=8, N=6).

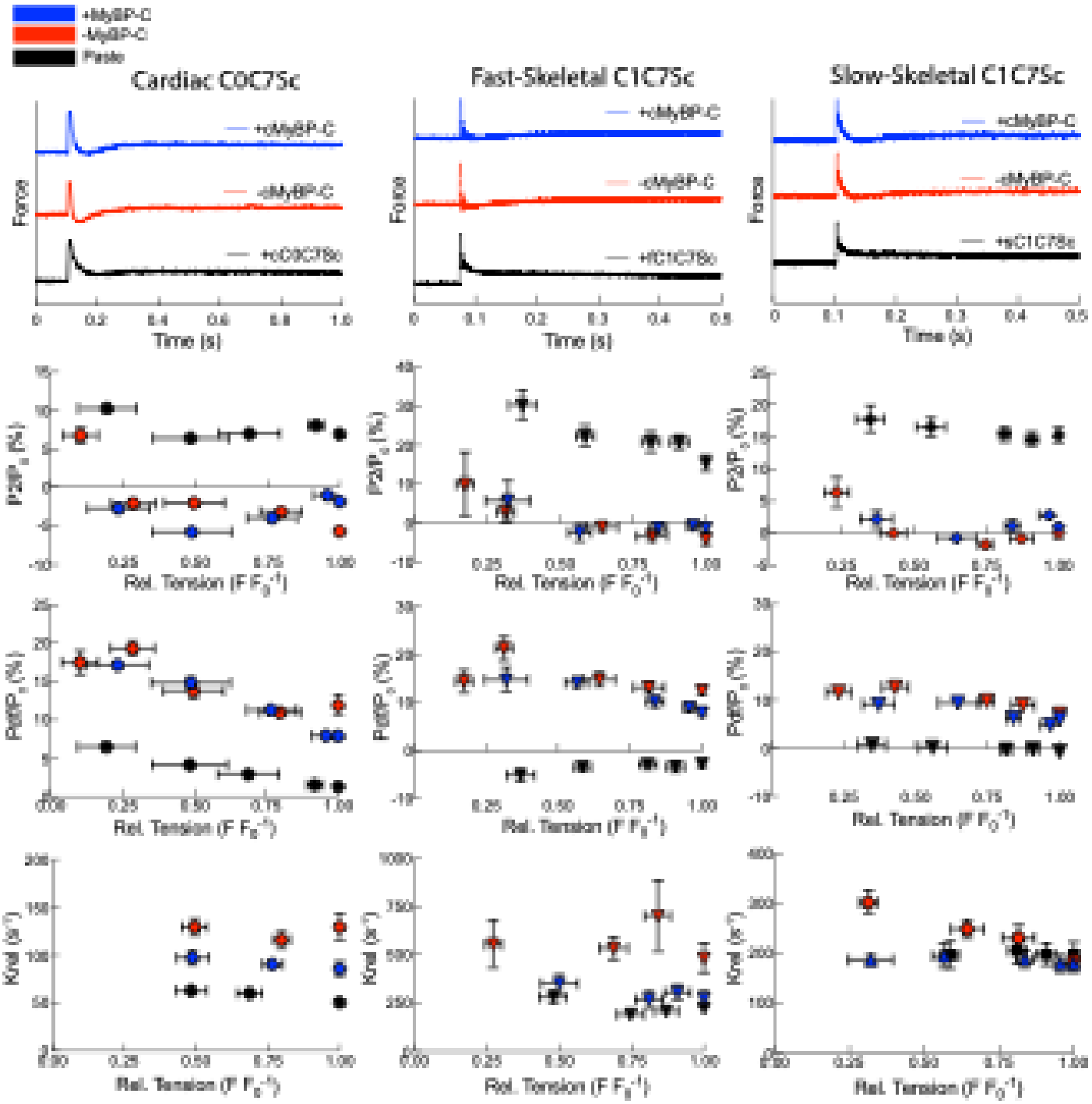


1038 **Figure 5**: Amplitudes of strain-induced cross-bridge detachment ($P_2$), stretch activation ($P_{df}$), and
1039 cross-bridge relaxation kinetics ($k_{rel}$) in cardiac muscle following *in situ* replacement with
1040 cC0C7Sc, fC1C7Sc, and sC1C7Sc. **a-c:** Representative force traces of cardiac tension transients
1041 before (blue) and after (red) removal of endogenous cMyBP-C, and following replacement
1042 (black) with recombinant cC0C7Sc (a) fC1C7Sc (b), and sC1C7Sc (c). **d-f:** Amplitude of strain
1043 induced cross-bridge detachment ($P_2$) before and after removal of endogenous cMyBP-C and

1044 after replacement with cC0C7Sc (d) (pCa*Treatment*pCa Prob > F = <0.0001), fC1C7Sc (e)
1045 (Treatment Prob > F = <0.0001), and sC1C7Sc (f) )(Treatment*pCa Prob > F = 0.0234) **g-i:**
1046 Amplitude of stretch activation ($P_{df}$) before and after removal of endogenous cMyBP-C and after
1047 *in situ* replacement with cC0C7Sc (g)(Treatment*pCa Prob > F = 0.0029), fC1C7Sc
1048 (h)(Treatment*pCa Prob > F = 0.0076), and sC1C7Sc (i)(Treatment*pCa Prob>F = 0.0181. **j-l:**
1049 Rates of stretch induced cross-bridge relaxation ($k_{rel}$) before and after removal of endogenous
1050 cMyBP-C and after *in situ* replacement with cC0C7Sc (j)(Treatment Prob > F = <0.0001), fC1C7Sc
1051 (k)(Treatment Prob > F = <0.0001), and sC1C7Sc (l)(Treatment*pCa Prob > F = 0.0076). Statistics
1052 throughout are an ANOVA design with pCa, treatment, and their interaction as main effects,
1053 including an individual fiber random effect. A post-hoc Tukey's HSD test was performed on
1054 statistically different main effects ($p < 0.05$). Dataset: cC0C7Sc (n=7, N=3), fC1C7Sc (n=6, N=5),
1055 sC1C7Sc (n=8, N=6).

1056

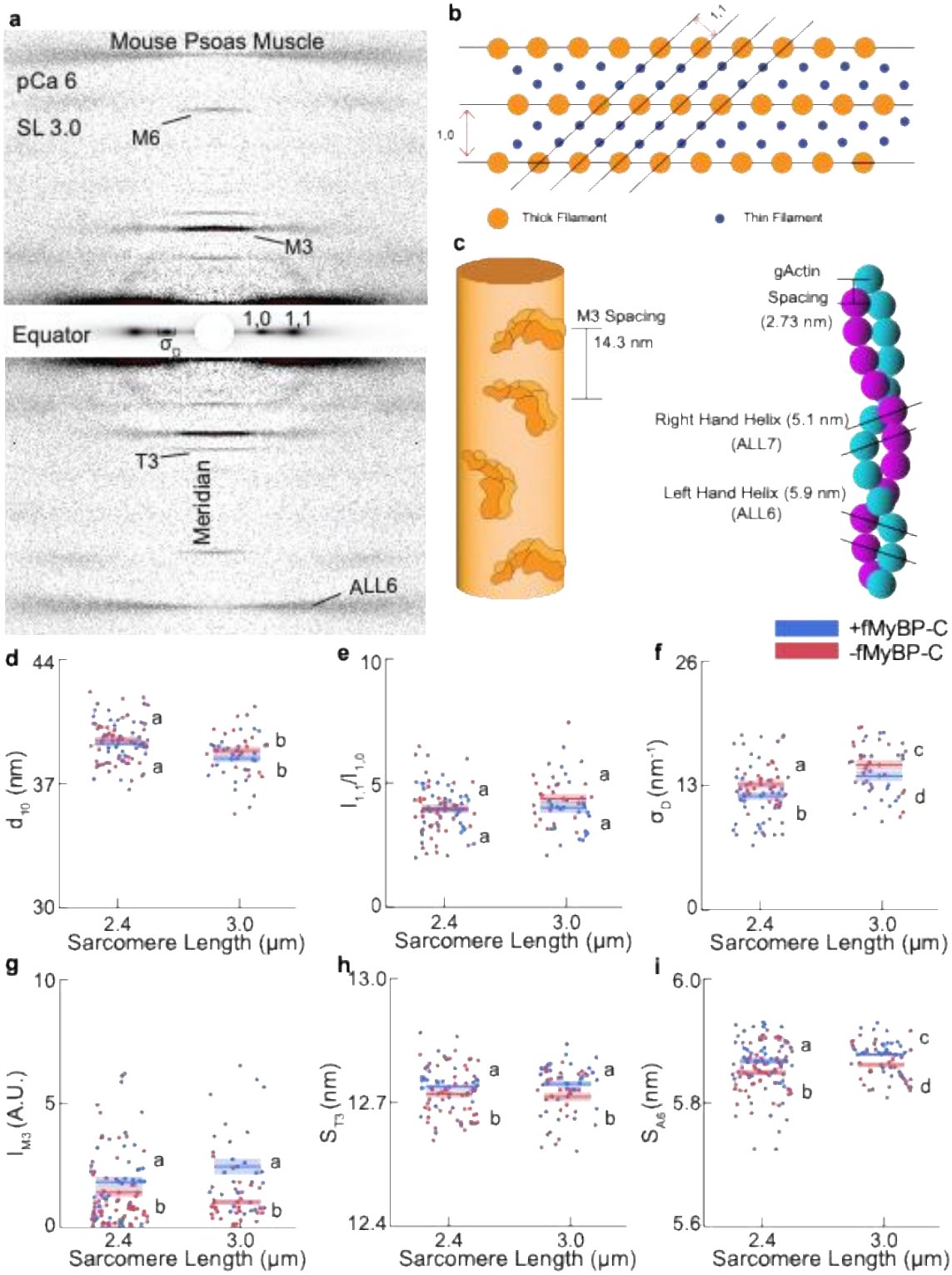


**Figure 6**: Equatorial and meridional reflections of isometrically contracting psoas Muscle in presence and absence of fMyBP-C. **a)** Representative X-ray diffraction image at SL 3.0 and pCa 6.0 highlighting meridional reflections (M3, T3, M6, A6) assessed in this study. **b)** Graphic

showing a cross-sectional view of the sarcomere lattice as well as important equatorial reflections. **c) Left:** Schematic of the quasi-helical arrangement of myosin heads on the thick filament backbone, where the M3 reflection is highlighted as difference in space between individual myosin crowns. **Right:** Schematic of the thin filament, highlighting both the left-handed and right-handed helix of the actin monomers and their spacings. **d)** Lattice spacing of permeabilized psoas muscle at SL 2.4 and SL 3.0 before and after removal of fMyBP-C (Treatment: Prob > F 0.1494) **e)** $I_{11}/I_{10}$ intensity ratio of permeabilized psoas muscle at SL 2.4 and 30 before and after removal of fMyBP-C. (Treatment: Prob > F = 0.2284) **f)** Heterogeneity of lattice spacing ($\sigma_D$) of permeabilized psoas muscle at SL 2.4 and 3.0 before and after removal of fMyBP-C. (Treatment: Prob > F = 0.003) **g)** Intensity of the M3 reflection ($I_{M3}$) of permeabilized psoas muscle at SL 2.4 and 3.0 before and after removal of fMyBP-C. (Treatment: Prob > F = 0.0001) **h)** T3 spacing ($S_{T3}$) of permeabilized psoas muscle at pCa 6.0 at SL 2.4 and 3.0 before and after removal of fMyBP-C. (Treatment: Prob > F = 0.0377) **i)** Actin layer line 6 spacing ($S_{ALL6}$) of permeabilized psoas muscle at SL 2.4 and 3.0 before and after removal of fMyBP-C. (Treatment: Prob > F = 0.0026) Statistics throughout are a repeated measure ANOVA design with SL, treatment, and their interaction as main effects, including a random effect on individual fiber. A Student's t-test or Tukey's HSD Post-Hoc test was performed on statistically significant differences and presented in figures as connecting letters. Dataset: (n=43 fibers, N=13 animals).